# Techno-economic evaluation of solar-driven ceria thermochemical water-splitting for hydrogen production in a fluidized bed reactor

Adetunji Onigbajumo[a,1], Priyanka Swarnkar[a,b], Geoffrey Will[a], Thirumalachari Sundararajan[b], Alireza Taghipour[a], Sara Couperthwaite[a], Ted Steinberg[a], Thomas Rainey[a]*

[a] School of Mechanical, Medical and Process Engineering, Queensland University of Technology, GPO Box 2434, Brisbane, QLD 4000, Australia

[b] Department of Mechanical Engineering, Indian Institute of Technology Madras, Chennai 600036, India

* Corresponding Author: t.rainey@qut.edu.au

## Highlights

- ASPEN Model of ceria thermo-reduction in fluidized bed reactor was developed.
- Economic potential of ceria based TCWS plant for hydrogen production is assessed.
- Solar PDC and PV-battery energy integration is economic for ceria TCWS hydrogen plant.
- MSP of hydrogen at 3.92 USD/kg $H_2$ is achieved with high potential for 2 USD/kg $H_2$.
- Carbon tax credit is an important incentive in economic solar-driven TCWS plant.

## Abstract

Thermochemical water splitting (TCWS) is an attractive and promising approach for hydrogen fuel production to replace fossil fuels and address climate change. The novel approach used in this study is the indirect irradiation of the ceria particle with solar-heated nitrogen in a fluidized bed reactor which improved the ceria thermo-reduction and increased hydrogen yield. The TCWS plant featured additional units for oxygen co-production, and excess heat recovery to generate electricity and reduce the saleable hydrogen price. Two fluidized bed reactors for ceria thermo-reduction and oxidation using steam were modelled in Aspen Plus for hydrogen production at a 70% capacity factor. A photovoltaic (PV)-battery module in addition to the solar parabolic dish collector (PDC) was then used to deliver operation-round electricity supply and drive mechanical and control systems, reducing overall plant energy cost. Three minimum selling prices of hydrogen were considered based on the achievable products of the TCWS plant: (i) pricing based on no co-products, (ii) pricing including oxygen revenue, and (iii) pricing including oxygen and electricity revenue. The TCWS plant achieved a minimum selling price (MSP) of 3.92 USD/kg $H_2$ (including oxygen and electricity revenue) at a 10% discount rate which is the lowest for solar-driven TCWS hydrogen compared with other similar studies. Sensitivity analyses showed that discount rate, steam Rankine cycle, power block, cost of ceria and hydrogen storage, and price of oxygen, respectively, had the highest impact on the MSP of the TCWS hydrogen plant. The switch value analysis (SVA) was used to determine the potential of achieving the global target hydrogen price of 2 USD/kg based on a single parameter assessment. The TCWS plant proposed in this work provides a promising approach toward achieving future hydrogen prices below 2 USD/kg when a lower discount rate of 5% is utilised. It was established that the choice and size of concentrated solar power (CSP) technology integration, co-generation, and heat recovery are critical to the system efficiency and economic viability of a solar-driven TCWS hydrogen production. This work demonstrated the use of ceria as a metal oxide feed suitable for solar TCWS hydrogen production with a promising economic potential for a global target price of less than 2 USD/kg $H_2$ based on the choice of process-CSP configuration.

**Keywords**: Thermochemical water splitting, Hydrogen, Ceria, Concentrated solar power, Aspen Modelling, Fluidized bed reactor, Techno-economics, Co-generation.

## Nomenclature

AUD – Australian dollar
BMC – Bare module cost
BMF – Bare module factor
CAPEX – Capital expenses

CEPCI – Chemical engineering plant cost index
CNTRL – Control
CRF – Capital recovery factor
CTC – Carbon tax credit
CYCLN – Cyclone
DCF – Discounted cash flow
DNI – Direct normal irradiance
DPI – Direct permanent investment
DPP – Discounted payback period
FBOR – Fluidized bed oxidation reactor
FBRR – Fluidized bed reduction reactor
FLW – Flow
GNRTR – Generator
HEX – Heat exchanger
IRR – Internal rate of return
LCOE – Levelized cost of energy
LCOH – Levelized cost of hydrogen
LT – Low temperature
MO – Metal oxide
MSP – Minimum selling price
NPV – Net present value
OPEX – Operating expenses
PDC – Parabolic dish concentrator
PSD – Particle size distribution
PV – Photovoltaic
RC – Rankine cycle
RCPRTOR – Recuperator
RCVR – Receiver
RTRN – Return
SAM – System Advisory Model
SEPRTR – Separator
SRC – Steam Rankine cycle
SV – Switch value
STRGE – Storage
TCI – Total capital investment
TCWS – Thermochemical water splitting
TDC – Total depreciable cost
TDH – Transport disengagement height
TPI – Total permanent investment
USD – United stated dollars
WC – Working capital
WTR – Water

**Symbols and units**
h – hour
kWe – kilowatt electricity
MWh – mega Watt hour
$MW_{th}$ – mega Watt thermal
t/h – tonnes per hour
J/kg.K – Joule per kg Kelvin
Pa.s – Pascal second
W/m – Watt per metre
y - year
V – velocity
C – Coefficient
Re – Reynolds
g – gravitational acceleration
d - diameter
Wdc – Watt direct current
kWh – kilowatt hour

**Greek letters**
$\rho$ – Density
$\mu$ - viscosity

**Subscripts and superscripts**
t – terminal flow
p – particle
g – inert gas
d - drag

## 1. Introduction

With the increasing global population comes a higher demand and consumption of materials and energy to ensure human survival. To deliver current global energy consumption requirements, there has been a reliance on fossil-based fuels [1]. However, the utilisation of fossil fuels has come with a high price in terms of greenhouse gas (GHG) emissions which has resulted in global warming [2,3]. There is a growing need to considerably reduce the over-dependence on fossil fuels and embrace renewable (green) energy so that $CO_2$ emissions will not lead to a 1.5 ºC rise in global temperature and a point of "no-return" [4,5]. If renewable energy utilisation will deliver a significant reduction in global warming, it must address industrial energy requirements and meet the need of the transport sector [3]. While solar energy is the most abundant and available renewable energy source, its exploitation and integration to achieved a less expensive alternative fuel is key to a sustainable green energy economy [3,6].

Hydrogen is one of the most amenable and utilisable future energy sources with minimal environmental challenges and high applicability for heating, nuclear, chemical, electrical, and transport energy [7]. Hydrogen as a

transport fuel doesn't emit particulate in the exhaust without emission exhaust and delivers more than 200% specific energy density of gasoline [8] with growing interest in the automobile industries for hydrogen fuel commercial cars [9]. In 2006 alone over 50 million Mt of hydrogen were produced globally with about a 9.8% annual increase [8,10]. The global demand for hydrogen either in its pure form or combined in other mixtures such as syngas, and fertilizers, is expected to reach 18% by 2050 [11]. Despite the potential for hydrogen utilisation, over 90% of global hydrogen production is fossil fuel-based with less than 5% from electrolysis and less than 1% from renewable energy sources [12,13] as shown in Fig 1. In addition, for hydrogen to displace fossil-based fuels, it must be in an easily transportable form [14,15], cheaper [14], and compatible with existing physical infrastructures and mechanical systems [16,17].

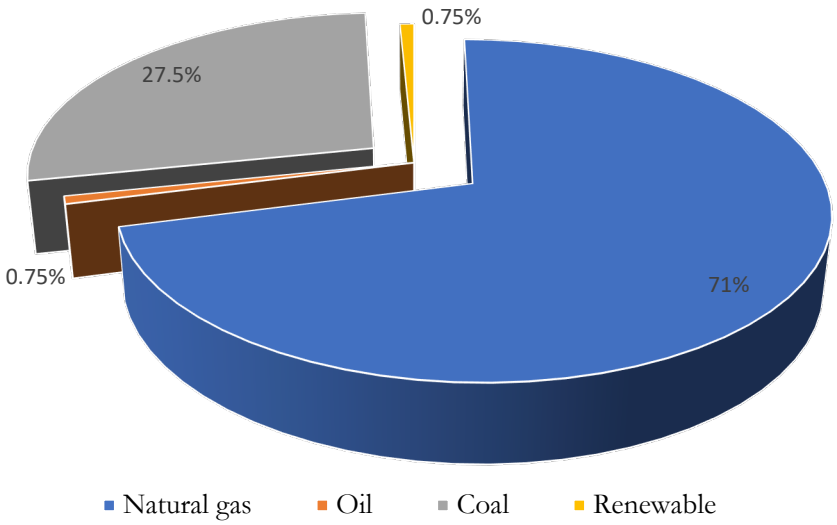


Fig. 1. Current energy sources for global hydrogen production in 2019 [7,12].

The production of hydrogen is dependent on two factors: raw material feed and energy source [7,18]. Natural gas reforming and coal gasification for hydrogen production are the most established thermal energy-driven hydrogen production pathways. In natural gas reforming for instance, for every 1 kg of $H_2$ produced, at least 5.5 kg of $CO_2$ is generated [8] which is the main challenge in the light of greenhouse gas emissions and a sustainable environment. Similarly, coal gasification which is common for hydrogen production and able to deliver a minimum hydrogen price of less than 2 USD/kg $H_2$ [8,17] is not suitable for mitigating global warming. Although the electrolysis of water has been around since the 18$^{th}$ century for hydrogen production, it is energy-intensive and may not be economic in locations where there is a high cost of electricity [19]. Even in locations where electricity is considered cheap, there is still a challenge of global warming when electrical energy is generated by fossil fuels. Photovoltaic-based water electrolyser for hydrogen production is a simpler option but is only able to utilise a small fraction of the light wavelength with many reaction steps which ultimately leads to lower system efficiency and high cost [8,20].

Thermochemical water splitting (TCWS) is similar to thermolysis (electrolysis by thermal energy) for hydrogen production which splits water into $H_2$ and $O_2$ [19]. However, unlike thermolysis which is a direct thermal dissociation of water, TCWS utilizes a two-step thermochemical reaction to reduce a metal oxide (MO) which is redox-active to release hydrogen [7]. The reduced metal oxide is then made to react with steam and re-oxidised by taking the oxygen from the steam and releasing hydrogen gas [8,16]. Studies on TCWS cycles began with Funk and Reinstrom [21] while Nakamura first developed a thermochemical cycle in 1977 [16,22] on the basis of stoichiometric redox-active metal oxides such as $Fe_3O_4$/3FeO, ZnO/Zn, CdO/Cd, and $CeO_2/Ce_2O_3$. While several studies [23,24] considered ZnO/Zn-based thermochemical cycle redox as having a significant thermodynamic advantage compared with most metal oxide redox pairs, it is still not industrially economic. ZnO thermochemical cycle is known for slow reaction kinetics, backward reactions, and high energy consumption for zinc-oxygen separation [24]. Research interest is increasing in the use of ceria as a redox-active MO being a promising material

for thermochemical redox cycles having stable crystal structure at extensive thermal cycling and increased oxygen release and deposition potential [25,26].

Two-step thermochemical cycles of metal oxides (MOs) are energy-intensive requiring up to 1500 ºC to reduce the MO to a non-stoichiometric oxide ($MO_{x-\delta}$), hence the reason why they are driven by concentrated solar thermal (CST) energy input [27]. Fig. 2 describes the solar-assisted TCWS of ceria to produce hydrogen with oxygen as a useful by-product. Recent works on TCWS of ceria had reported low efficiencies of the reactors due to the high endothermic reaction involved [28,29]. The ease of accumulation of MO in the reactor chamber with a high potential of the particle damaging the optical receiver component is a major challenge with solar thermochemical reduction of MOs such as ceria. This is in addition to the limited reduction extent (δ) at both the upper and lower end of reduction temperatures of oxygen partial pressures, during the thermochemical process [30].

The thermochemical cycle of MOs is still a growing field of research with limited studies, especially on TCWS of ceria. The stability of ceria over extensive thermal cycles had been investigated extensively [31–33]. Doping of ceria with other MOs as catalysts has been studied with findings that suggested increased reaction sites and improved kinetics [34–36]. Most studies available on solar-driven TCWS for synthetic fuel production have also focused on the technical feasibility of the technology on a laboratory scale [37–39]. However, common to all these studies, irrespective of the solar reactor choice is lower process conversion and yield due to the direct heating of the MO in the reactor chamber [25,40,41]. Overall, these challenges with the cost of CST energy utilization contributed to the huge cost of hydrogen production per kg via TCWS technologies compared to the U.S. DOE target cost of 2 USD/kg $H_2$ [31].

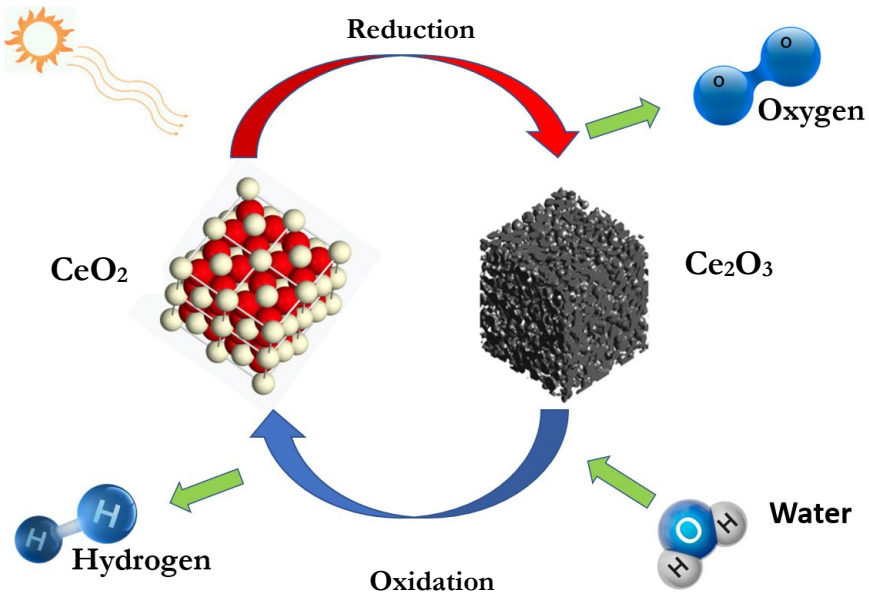


Fig. 2. Schematic of a solar-assisted thermochemical water splitting of ceria.

Despite the potential of hydrogen production via thermochemical water splitting, there are very limited studies on the economic assessment of TCWS with ceria as metal oxide. In the studies of Moser et al., [41], CST-based TCWS of ceria in comparison with nickel-ferrite oxide was assessed. The study reported 13.06 €/kg $H_2$ and 38.83 €/kg $H_2$ with ceria and nickel-ferrite oxide, respectively. Also, in the study of Budama et al., [31], solar-driven TCWS of ceria for hydrogen and CO co-production was evaluated. A promising minimum selling price (MSP) of hydrogen was reported at 4.55 USD/kg $H_2$ with electricity co-generation. Similarly, in the study of Restrepo et al. (2022) [42], hydrogen production cost of 4.6 USD/kg $H_2$ was obtained for high-temperature electrolysis and 4.32 USD/kg H2 for metal oxide cycle system. The metal oxide modelled in the study of Restrepo et al. (2022) was however generic and challenging to utilise for economic comparisons due to differences in reaction activity and the extent of non-stoichiometry of different MOs. Common to all the available studies in the utilisation of heliostat-based CST technology which resulted in a significant contribution to the total plant cost and increased the selling price of hydrogen. For instance, in the study of Farooqui et al., 2019, the solar field and tower made up 39% of the equipment cost [2]. This therefore highlights the need to try alternative solar thermochemical hydrogen production pathways. the economic performance of a TCWS through indirect radiation of ceria particle in a fluidized bed

reactor which is not available to the author's knowledge. Also, based on the available literature, no study has achieved MSP closest to the global hydrogen price target of 2 USD/kg $H_2$. Hence, the objective of this study was to present a steady-state ASPEN Plus model of an indirect solar-driven ceria TCWS plant with an evaluation of the economic potential of the commercial-scale size hydrogen production, oxygen gas, and electricity co-generation. The minimum selling price (MSP) and levelized cost of hydrogen (LCOH) were estimated and compared to determine the economic viability of the approach considered in this study.

This work demonstrated a novel TCWS process modelling with fluidized bed reactor using ASPEN Plus by achieving thermochemical reduction through indirect solar irradiation of ceria particle with hot nitrogen. In addition, continuous PV-battery module-based supplementary electricity was integrated to drive machinery and control systems of the TCWS hydrogen plant. Furthermore, this study presents a novel approach to solar thermochemical hydrogen production using an ASPEN-based model without external sub-routine codes. This is achieved by computing critical parameters such as bed inventory, elutriation, transport disengagement height (TDH), fluidization velocity, and gas distribution and utilising them for the reactor model in ASPEN.

This work presents an economic and low environmental impact alternative for hydrogen production with renewable energy such as solar thermal energy and indirect water splitting. This approach (solar thermochemical hydrogen production) offers a good potential for green hydrogen and delivers a significantly lower impact on the environment compared to the conventional route via electrolytic and natural gas reforming which are fossil fuel driven. To the authors' knowledge, no previous study had attempted to model the indirect solar thermochemical hydrogen production with a fluidized bed reactor with ASPEN Plus without the need for an external subroutine code for the fluidisation process. Previous studies instead considered direct solar hydrogen production using a heliostat based solar tower to drive the thermochemical reactor. This work therefore provides a pathway for techno-economic assessment of ASPEN-based metal oxide thermo-reduction and water splitting process modelling with fluidized bed reactor in the future. The comparison between the hydrogen MSP in this work with similar studies on the production of hydrogen was presented while sensitivity and switch value analysis provide the cost reduction opportunities and future economic realities.

## 2. Methodology

Fig. 3 shows the block diagram for the TCWS of ceria particles using an indirectly solar irradiated fluidized bed reactor for hydrogen production. The process heat for the plant was delivered by a parabolic dish solar concentrator and a volumetric receiver arrangement to drive the fluidized bed reactors as they are both energy intensive requiring temperatures up to 1200 ºC [3]. The solar field arrangement was modelled using the System Advisory Model (SAM) program. The overall process plant sized at 22.4 Mt/y of ceria throughput comprising a fluidized bed reduction reactor (FBRR) and oxidation reactor (FBOR), solid-solid heat recuperator, solid-gas cyclone, heat exchanger, steam generator, gas separator, control flow valve, vacuum pump, particle mixer, hydrogen, and oxygen storage tanks. The TCWS of the ceria feedstock was modelled in ASPEN Plus software based on the approach of Wei et al., [43] using nitrogen as the heat transfer gas for indirect irradiation of the ceria particle in the reduction fluidized reactor.

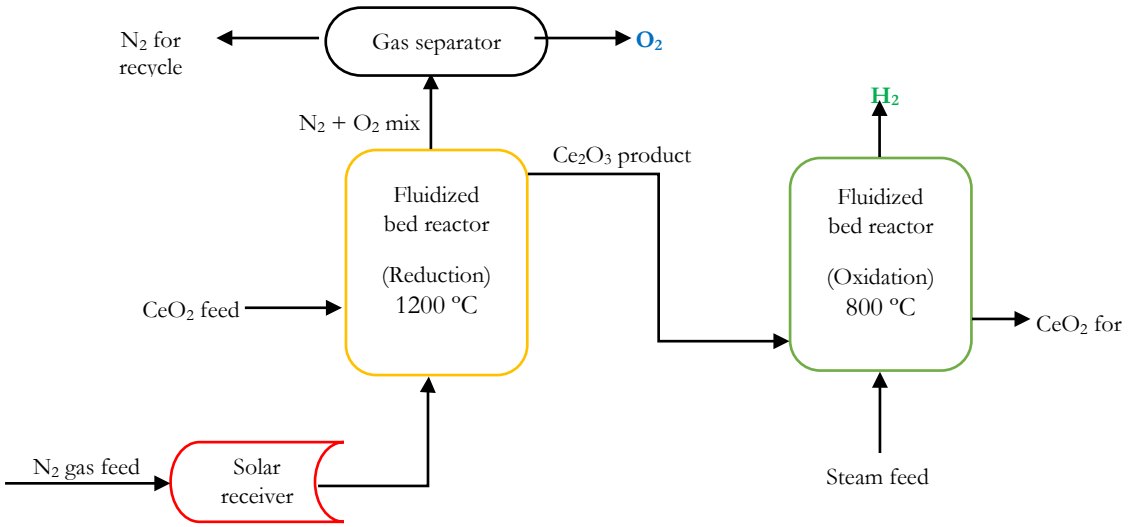


Fig. 3. Block diagram for the TCWS of ceria particle for hydrogen production.

The process configuration considered the recovery and utilisation of significant process heat within the system and channel flow exergy to the FBOR to enhance process conversion, hydrogen yield, and plant energy efficiency. To minimise the size of the solar energy resource and the energy consumed by the fluidized bed reactors, the overall process configuration utilized a heat recovery loop using recuperators and heat exchangers where possible. Pumps and other electrical control systems in the plant were powered by a photovoltaic (PV) based solar field arrangement. Detailed process and modelling descriptions are provided in the next sub-section. Thermodynamic data, conventional solid material behaviour, hydrodynamics, physical and chemical properties were based on Aspen Plus V.9 and other relevant sources. Energy requirements to account for solar thermal heat delivered by the solar field component modelled in SAM were based on component sizing, ratings, and energy calculations from Aspen Plus evaluations.

## 2.1 Component descriptions

The fluidized bed reactors were used for the reduction and oxidation of the ceria particle to produce cerium (III) oxide ($Ce_2O_3$) and ceria ($CeO_2$) outputs, respectively. The details of nitrogen-ceria particle heat transmission are not within the scope of this study. For simplicity, heat loss between solid-gas-reactor interactions was considered negligible. Residence time and particle exiting were based on the study of Wei et al. [43] with a consideration of temperature probe usage for homogenous temperature within the reactor. Pressure swings were controlled within the reactors theoretically based on the minimum flow rate estimate of the nitrogen gas controlled by the gas pressure valve [2,43]. Gas separators were used for nitrogen-oxygen gas separation for FBRR products and hydrogen-steam separation for FBOR products. The gas-solid cyclones were installed to collect and retain particles that escape with gases in the freeboard of the fluidized bed reactor when reduction is complete. The cyclones were connected to the FBRR and FBOR through the vacuum pumps which entrained the gas-particle mixture and flow into the cyclones.

A solid-solid heat recuperator was considered to recover radiant heat from the hot ceria particle returning from the FBOR which in turn was used to preheat the refill ceria particle used to maintain a constant material feed in the plant throughout the production cycle. The heat recuperator design was based on that used by Budama et al., [31] with the model assuming a heat exchanger-based radiation heat transfer around the heated tubes in the recuperator. Thermal energy transfer between particles in the recuperator is a function of the view factor and emissivity which is assumed unitary and taken not to impact the efficiency of the system when other variables are applied.

Heat exchangers were modelled using the minimum temperature approach at design calculation mode with a counter-current flow direction. Steam generators were utilised to recover excess radiant heat from (i) the ceria particle exiting the FBRR (ii) ceria particle exiting the solid-solid recuperator. In the first case of the steam generation, the steam was used in the FBOR for reoxidation of cerium (III) oxide, while in the second, the steam was used for the turbine in the Rankine cycles. The design of the steam generator and its sub-components: super-heater, evaporator, and economizer, with regards to thermal radiation resistance and view factor were based on the study of Budama et al., [31].

## 2.2 Process Description

The process flow diagram for the TCWS plant for hydrogen production with oxygen and electricity co-generation is shown in Fig. 4. Ceria particles (assumed to have spherical shape) were fed into the fluidized bed reactor through a conveyor system at 80 t/h and indirectly irradiated with solar-heated inert gas through the reactor. The inert gas was heated by the solar radiant heat from a parabolic concentrator focused on a volumetric receiver which holds the gas until it reached a minimum of 1200 ºC. The parabolic solar concentrator and a ceramic-based volumetric receiver were considered because of their high concentration ratio and ability to supply hot gas above 1300 ºC, respectively [44,45]. The ceria particles were reduced in the FBRR with oxygen gas being released while the inert gas was used to sweep the oxygen off the freeboard using a vacuum pump into the cyclone. The cerium (III) oxide (reduced ceria) exited the fluidized bed reactor at the solid discharge location. The ceria-cerium (III) oxide reduction/oxidation reaction is as follows:

$$2CeO_2 \rightarrow Ce_2O_3 + 0.5O_2 \text{ (reduction)} \quad (1)$$

$$Ce_2O_3 + H_2O \rightarrow 2CeO_2 + H_2 \text{ (oxidation)} \quad (2)$$

The gaseous mix in the cyclone was sent to a flash separator where oxygen was separated, cooled, and sent to storage while the hot inert nitrogen gas returned to the solar volumetric receiver where it was reheated and re-used in the FBRR. The high-temperature cerium (III) oxide particle was first sent to a steam generator where

sensible heat from the particles transfers to the cold-water stream while the cerium (III) oxide proceeded to the FBOR at 800 ºC. To achieve superheated steam for re-oxidisation in the FBOR, the hot water from the steam generator was sent to a heat exchanger which recovers the excess heat from the gas mix from the FBRR-cyclone. The superheated steam was then sent to the FBOR reactor where cerium (III) oxide was re-oxidized to ceria giving off hydrogen with a mix of vapour in the freeboard.

The hydrogen-vapour mixture was passed into a second separator where hydrogen was obtained free while the vapour was used as inlet steam for the steam Rankine cycle (SRC). To ensure a constant supply of steam to the ORC for electricity production, sensible heat from the produced oxygen was recovered for steam generation while the oxygen was stored at a lower temperature. Some of the sensible heat in the hydrogen gas product was also recovered by preheating the nitrogen gas exiting the process prior to its re-entry into the volumetric solar receiver. The ceria (oxidized cerium (III) oxide) exited the fluidized bed reactor while the sensible heat from the particle was recovered through a solid-solid recuperator to preheat the make-up ceria particle used to maintain the ceria feed rate. This was to minimize the thermal differential between the make-up ceria as a cold particle mixed with the hot ceria particle to be re-used in the FBRR. The solid-solid and solid-gas phase exchanger effectiveness was taken as 0.8 [2].

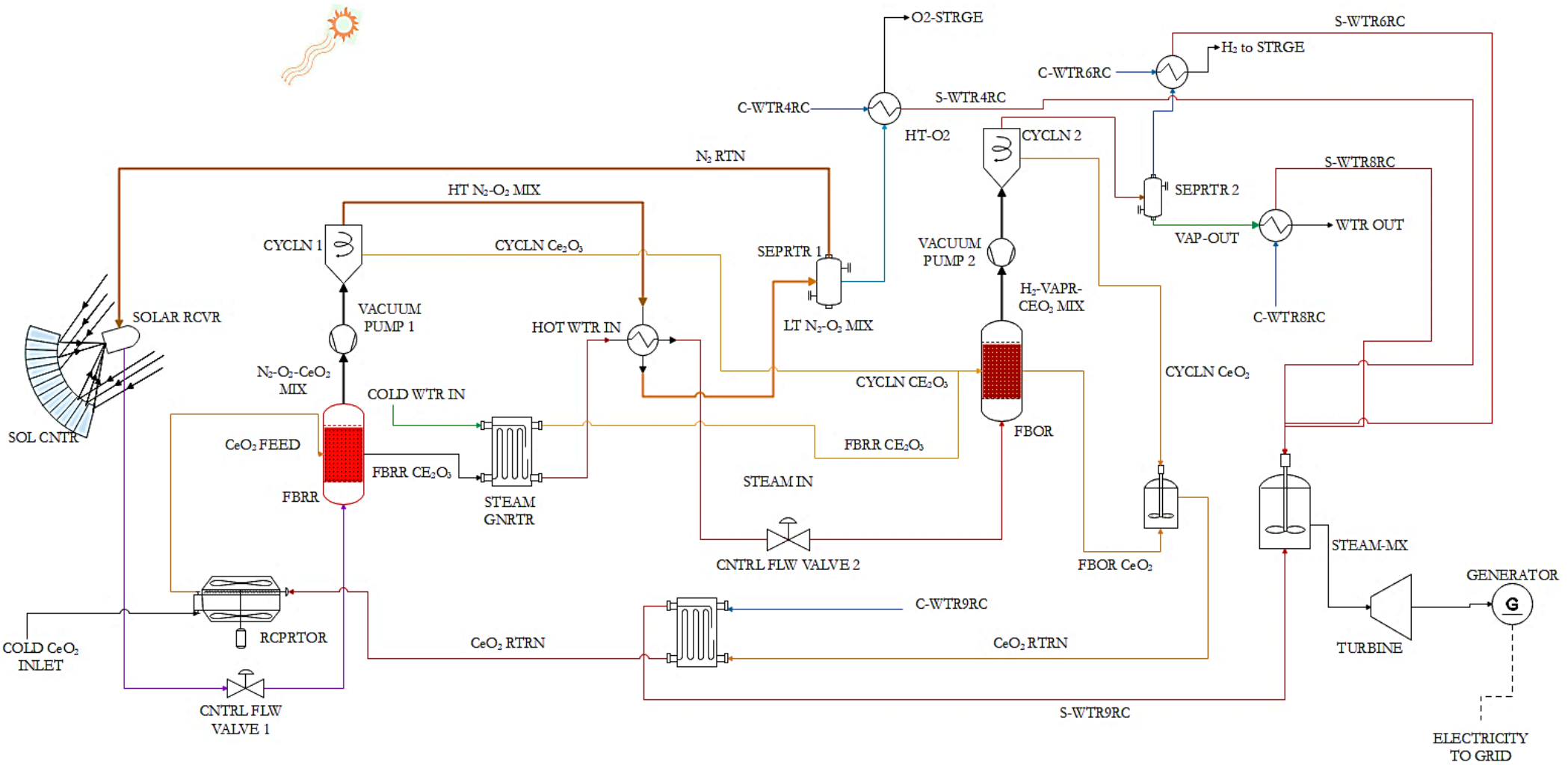


Fig. 4. Schematic flow diagram of the indirectly irradiated solar-assisted TCWS of ceria particle for hydrogen and oxygen co-production.

The choice of fluidization reactor and thermo-reduction for the TCWS process in this work was to ensure a maximum endothermic reaction, inter-particle contact, and heat transfer between the solid-gas phases. The particles ($CeO_2$/ $Ce_2O_3$) were made to settle in the reactor bed with the nitrogen gas blown at sufficient fluidization velocity (Eq. 3) to allow heat transfer throughout the particle. Terminal flow velocity ($V_t$) required for fluidization was determined to be:

$$V_t = \sqrt{\frac{4(\rho_p - \rho_g) g d_p}{3 C_d \rho_g}} \quad (3)$$

Where $\rho_p$ is the density of ceria (solid), $\rho_g$ is the density of inert gas, $g$ is the gravitational acceleration, $d_p$ is the diameter of ceria particle, and $C_d$ is the drag coefficient.

The drag coefficient is given by:

$$C_d = \frac{a+b}{Re} + \frac{c}{Re^2} \quad (4)$$

Where Re is the Reynolds number at terminal velocity, a, b, and c are empirical constant 1.22, 29.17, and 3.9, respectively. The Reynolds number is calculated as:

$$Re = \frac{d_p V_t \rho_g}{\mu} \quad (5)$$

Where $\mu$ is the kinematic viscosity of nitrogen at the inlet temperature in the fluidized bed reactor.

## 2.2 ASPEN Plus modelling

The TCWS using a reduction and oxidation fluidised bed reactor was modelled in Aspen Plus v10. The fluidized bed reactor as introduced in Aspen Plus v10 had been validated extensively for various processes in the literature [46,47]. The ASPEN Plus property method (Equation of State) and base methods used is the SOLIDS. Table 1 presents the assumptions and other relevant data used in the model development as obtained from the literature. The ceria particles ($CeO_2$ FEED) were heated in the FBRR when it came in contact with the solar irradiated inert gas for which nitrogen was used in this study. The flow rate of the nitrogen gas ($N_2$-IN) was estimated based on the requirement for fluidization of the ceria particles with the terminal velocity calculated based on Eq. 3. The operational flow velocity of nitrogen is about five times the minimum fluidization velocity with the correlation calculation based on Ergun [48,49]. The transport disengagement height (TDH) model was based on George and Grace [50,51] and the distributor pressure drop was according to Geldart classification B [52,53]. The elutriation model was also based on the Extended Geldart correlation [54,55]. Table 1 shows the assumptions and correlations utilised for this model. The thermal energy released by the nitrogen gas was assumed to be equal to the amount of heat transfer between the solid-gas phases. Reactor efficiency is equal to the ratio of heat absorbed by ceria particles in the reactor to the heat absorbed by the nitrogen in the solar receiver. Phase equilibrium conditions of the FBRR were considered as isobaric and isenthalpic for inlet nitrogen gas and isobaric and isothermal for the outlet gas mixture. The ceria particles were assumed to be homogeneous and ideal in the mix.

While 80 t/h ceria particles were bubbled in the FBRR with the hot nitrogen gas flow (1.24 t/h), oxygen was released into the freeboard while $Ce_2O_3$ (FBRR-$Ce_2O_3$) was produced and discharged based on the discharge height correlated with the TDH. The released oxygen mixed with nitrogen and entrained the $CeO_2$/$Ce_2O_3$ particles which escaped into the freeboard as $N_2$-$O_2$-$CeO_2$ MIX and were sucked out based on pressure difference by the vacuum pump (VACUUM PUMP 1) into the cyclone (CYCLN 1). In CYCLN 1, the high-temperature gas mix (HT $N_2$-$O_2$ MIX) wase being separated from the CYCLN-$Ce_2O_3$ particle and recovered at the solid discharge outlet. The reduced ceria (FBRR-$Ce_2O_3$) was sent to a steam generator where the sensible heat from the FBRR-$Ce_2O_3$ stream was used to preheat the inlet cold water (COLD WTR IN) stream with the solid particle stream exiting at 800 ºC. The CYCLN-$Ce_2O_3$ was sent directly to the FBOR while the HOT $N_2$-$O_2$ MIX was used to further heat the inlet water to achieve superheated steam (above 500 ºC) for the FBOR. The HOT $N_2$-$O_2$ MIX exits the HEX1 at a lower temperature as LT $N_2$-$O_2$ MIX. The LT $N_2$-$O_2$ was sent to the separator (SEPRTR 1) to obtain nitrogen and oxygen gas at different outlets, both exiting at 670 ºC. Sensible heat from the nitrogen and oxygen gas was recovered through HEX2 and HEX3, respectively to generate steam for the SRC electricity generation with the V-WTR2RC and V-WTR4RC. Further detail about the SRC is provided in the next section The nitrogen gas exiting HEX2 at 109 ºC was sent back to the volumetric solar receiver where its being reheated and reused in the FBRR. The oxygen gas from HEX3 flows to an oxygen tank where it was cooled and stored under pressure to be sold as compressed oxygen.

The physical, heat transfer, and fluidization phenomena of the FBOR are similar to the FBRR with the cerium (III) oxide particle being fluidized by the superheated steam (STEAM-IN) in the reactor. A mixture of hydrogen gas, vapour, and entrained $CeO_2/Ce_2O_3$ particles were collected at CYCLN to obtain a particle-free gaseous phase mixture. The particles were collected over time and mixed with the oxidized cerium (III) oxide (FBOR-$CeO_2$) which then returns as the inlet ceria particle feed passing through the solid-solid recuperator to the FBRR as explained earlier. The hydrogen gas was separated from the vapour in the separator unit (SEPRTR 2) with the heat from the hydrogen gas stream exiting at 1000 ºC recovered using HEX4 to generate steam (V-WTR6RC) for the SRC. The sensible heat in the vapour was also recovered at the HEX5 to generate additional steam (V-WTR8RC) for the Rankine cycle. The hydrogen gas exited the hydrogen tank and was stored away under pressure to also be sold as compressed hydrogen. Table 1 presents the assumptions and other relevant data used in the model development as obtained from the literature.

Table 1. Summary of process model inputs and assumptions for the TCWS process.

| Parameter | Value | Unit | Ref. |
|---|---|---|---|
| **Plant capacity (based on ceria particle processing** | 80 | t/h | |
| **Thermodynamic and transport properties** | SOLIDS | | [43] |
| **Isentropic efficiency** | 80 | % | |
| **Operation period** | 350 | days/year | |
| **Particle size distribution** | 250-300 | µm | |
| **$N_2$ flow rate in FBRR** | 1500 | kg/h | |
| **Specific heat capacity of $N_2$** | 1215 | J/kg.K | |
| **Initial temperature of $N_2$ entering receiver** | 25 | ºC | |
| **Average exit temperature of $N_2$ leaving receiver** | 1200 | ºC | [43] |
| **Viscosity of $N_2$** | $4.85 \times 10^{-5}$ | Pa.s | |
| **Minimum fluidization velocity of $N_2$** | 0.07 | m/s | [41] |
| **Density of $N_2$** | 0.268 | $kg/m^3$ | |
| **Thermal conductivity of $N_2$** | 0.07 | J/m.K | |
| **Specific surface area of ceria** | 10 | $m^2/g$ | [43] |
| **Specific heat capacity of ceria** | 460 | J/kg.K | |
| **Density of ceria** | 7220 | $kg/m^3$ | |
| **Diameter of ceria particles** | 300 | µm | [43] |
| **Initial temperature of ceria** | 25 | ºC | |
| **Steam flow rate in FBOR** | 4173 | kg/h | |
| **Mass of ceria particle return through recuperator** | 79791 | kg/h | |
| **Average amount of heat produced from steam generation** | 107.8 | $MW_{th}$ | |
| **Electricity consumed for plant process (from generation)** | 8 | MWh | |
| | | | |
| **Reactor** | | | |
| **Elutriation model** | Extended Geldart Classification | | [52–54] |
| **Transport disengagement height** | George & Grace | | [50,51] |
| **Minimum fluidization velocity** | (based on Ergun's correlation) | | [43,49] |
| **Voidage at minimum fluidization** | 0.6 | | |
| **Height of reactor** | 13.5 (FBRR), 7.5 (FBOR) | m | |
| **Circular diameter** | 2 | m | |
| **PSD type** | Gates Gaudin Schuhmann | | |
| **Dispersion parameter** | 250 (minimum) | | |
| **Maximum orifice diameter** | 300 | µm | |
| **Approximate surface area of reactors** | 92 | $m^2$ | |
| **Distributor design** | Perforated plate | | |
| **Cyclone design** | Barth 4 – spiral inlet | | |
| **Underflow diameter** | 0.75 | m | |
| **Vortex finder** | 1.13 | m | |
| | | | |
| **Solar Field (Parabolic Dish Collector)** | | | |
| **Solar DNI** | 950 | $W/m^2$ | [3,43] |
| **Number of collectors** | 48 | | |
| **Solar field area** | 10800 | $m^2$ | |

| | | | |
|---|---|---|---|
| **Approximately projected mirror area** | 91 | $m^2$ | |
| **Receiver aperture (diameter)** | 0.184 | m | |
| **Efficiency of concentrator/volumetric receiver** | 80 | % | [43] |
| **Thermal generation capacity** | 36 (approx.) | $MW_{th}$ | |
| **Solar field (PV-based electricity)** | | | |
| **Design nameplate DC capacity** | 9.3 | MWh | |
| **Module** | 3000 | Units | |
| **Nominal efficiency** | 19 | % | |
| **Battery storage** | 16 | h | |
| **Cells per module** | 96 | | |
| **Tracking and orientation** | Azimuth axis | 45 deg (TRL) | |
| **Solar field area** | 40.3 | acres | |
| **Ground coverage ratio** | 0.3 | | |
| **Solar Field (Power cycle)** | | | |
| **Design thermal input power** | 107.67 | $MW_{th}$ | |
| **Cycle efficiency** | 50.11 | % | |
| **Power cycle electricity generation** | 45.52 | MWe | |
| **High pressure turbine (inlet turbine)** | 160 | bar | |
| **High pressure turbine (outlet pressure)** | 40 | bar | |

## 2.3 Process energy integration

Due to the significant energy requirement of the thermo-reduction process, solar energy has been widely considered as a viable energy option with solar-to-fuel conversion efficiency and economic potential known as key measuring factors. The amount of solar insolation available in Australia, for instance, gives it an economic justification and potential in the world for CST-based hydrogen production via thermo-reduction water splitting as considered in this study. The solar field in this work was modelled in NREL SAM v(2018.11.11) which is input from the ASPEN Plus model of the TCWS process. Presented in Fig. 5 is the energy balance across the whole TCWS process plant.

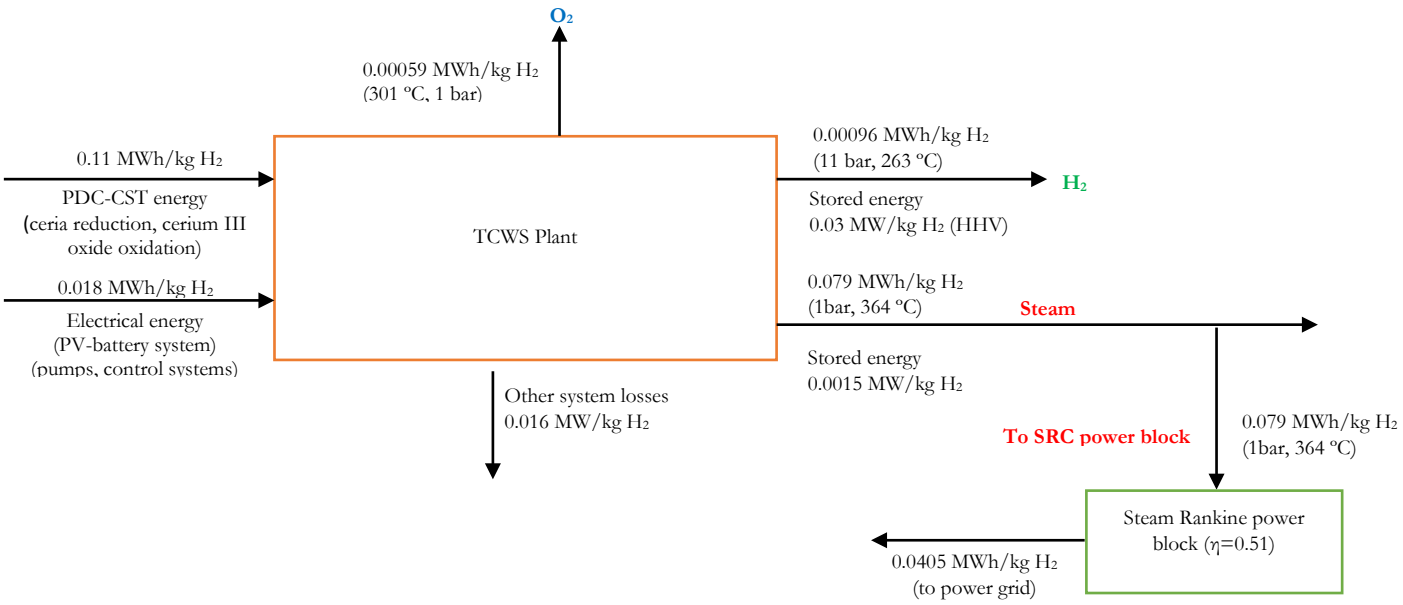


Fig. 5. Energy flow diagram for the TCWS and SRC power block electrical energy co-generation.

The solar field is divided into three parts: PDC for plant reactors, PV-battery system for pumps and electrical control systems, and SRC power block for electrical energy generation. The PDC solar field consists of a total of 48 parabolic dish collectors (PDC) with a total solar field area of 10800 $m^2$ with the system capacity based on the nameplate output of each collector arranged in series. The projected mirror area was approximately 91 $m^2$ at

a reflectance of 0.94 and receiver aperture diameter of 0.184 m. Direct normal irradiance of 950 W/m$^2$ was considered based on the annual solar insolation model of Northern Queensland (Townsville 19º 15´23´S 146º 49´6´E) in the author's previous study [3] with insolation cut-in of 200 W/m$^2$. The PDC solar thermal field arrangement as modelled in SAM produced approximately 46 $MW_{th}$ with output thermal energy of about 37 $MW_{th}$ at 80% thermal conversion efficiency of the concentrator [43]. The solar energy requirement to drive the fluidized bed reactors (reduction and oxidation) is 25.1 $MW_{th}$ with the average energy utilisation (including solar field losses) per kg hydrogen produced is 79kWh.

The electrical energy utilised for the pumps and control systems in the plant was driven by a 9.3 MW solar PV module solar field arrangement with up to 16 hours of battery storage for the non-solar hours. The PV module nominal efficiency is 19% with 96 cells per module. The PV solar field has a ground coverage ratio of 0.3 for an Azimuth axis tracking design with a tracker rotation limit of 45 degrees.

The steam Rankine power cycle was also modelled based on the relevant energy data from the Aspen Plus model detailing the thermal energy achievable from the heat recovered from the HEXs for steam generation (see Table 1). An average of 36.9 MWh was achieved by the turbine gross output design and net electrical energy output was 18.7 MWh at rated cycle efficiency of 0.51. The power cycle is an air-cooled condenser type with the high-pressure turbine inlet and outlet pressure are at 16 MPa and 4 MPa, respectively.

## 3. Techno-economic assessment

The economic feasibility of the TCWS plant was assessed by taking into accounts the results of the process model with the outcome of mass and energy balance from the Aspen Plus modelling to estimate the capital and operational costs. Three pricing scenarios: (i) no co-products (ii) oxygen co-product and (iii) oxygen and hydrogen co-products were considered based on the revenue achievable from the TCWS plant modelled in this work. The plant was assumed to operate during the solar active period of the day at an average of 10-hour period, as such electricity generation from the process plant through the SRC is stored. In the non-solar period (12-14 hours of the day), the electricity generated is used to drive the process plant and the shortfall is compensated for from the stored electricity sold to the grid. The economic analysis included the process plant estimates, the solar field cost, the SRC power plant for cost estimates while revenue included the selling price of hydrogen, oxygen, and electricity products of the overall plant design. The discounted cash flow analysis (DCF) was determined on the basis of the total capital investment, operations and maintenance cost using the bare module cost (BMC) approach [3,54] (see Table 2). The bare module cost approach was considered as it provides a robust approach for capital cost estimates. Net present value (NPV), internal rate of return (IRR), and discounted payback period (DPP) are calculated based on the DCF analysis. The plant profitability analysis was based on the 2019 US dollars (USD) while adjustments were made for comparisons with previous studies depending on the currency and year adopted in such work. Levelized cost and minimum selling price are used as indexes to evaluate the economic potential of the overall plant design with revenue analysis for 30 years of plant life. To project different economic scenarios and profitability measures, the sensitivity and switch-value (SV) analyses were considered.

Table 2. Assumptions of the bare module cost estimate [3,56].

| Cost item | Symbol | Estimate |
|---|---|---|
| Total bare module cost of equipment | $C_{FE}$ | $*C_{FE} = \sum_{i=1}^{n} X_i$ x BMF |
| Total bare module cost for related process machinery | $C_{PM}$ | |
| Total bare module cost for spares | $C_{spare}$ | |
| Total bare module cost for storage and tanks | $C_{storage}$ | |
| Total cost for initial catalyst charges | $C_{catalyst}$ | |
| Total bare module cost for computer systems, control system and instrumentation | $C_{comp}$ | |
| Total bare module investment ($C_{TBM}$) | | $C_{TBM} = C_{FE} + C_{PM} + C_{spare} + C_{storage} + C_{catalyst} + C_{comp,ctrl}$ |
| Cost of site preparation ($C_{site}$) | | $C_{site} = 0.15C_{TBM}$ |
| Cost of service facilities ($C_{serv}$) | | $C_{serv} = 0.2C_{TBM}$ |
| Total direct permanent investment ($C_{DPI}$) | | $C_{DPI} = C_{TBM} + C_{site} + C_{serv} + C_{alloc}$ |
| Cost of contingencies and contractor's fee ($C_{cont}$) | | $C_{cont} = 0.18C_{DPI}$ |
| Total depreciable cost ($C_{TDC}$) | | $C_{TDC} = C_{DPI} + C_{cont}$ |
| Cost of land, royalties | | $C_{land}$, $C_{royal} = 0.02C_{TDC}$ |
| Cost of plant start-up | | $C_{startup} = 0.1C_{TDC}$ |

| | |
|---|---|
| Total permanent investment (working capital, depreciable cost, land, royalties) | $C_{TPI} = C_{TDC} + C_{land}, + C_{startup}$ |
| Working capital ($C_{WC}$) | $C_{WC} = 0.15C_{TPI}$ |
| Total capital investment ($C_{TCI}$) | $C_{TCI} = C_{TPI} + C_{WC}$ |

*$X_i$ is the purchase cost of equipment item in USD, BMF is the bare module factor.

### 3.1 Capital and operating costs

The details of the plant process design based on each unit operation were used to estimate the capital and operating costs. Total capital investment includes equipment and installation costs, land purchases for TCWS plant, solar field and power cycle, site preparation, plant start-up, depreciable cost, and working capital. The fluidized bed reactor costing includes the reactor shell, distributor, tubes, mesh and bed plates, and insulation lining. Estimates are obtained using cost databases [57,58] plant design and cost estimation books [59], and relevant literature [31,60]. Component costs were obtained by multiplying equipment cost with the bare module factor (BMF) (see Table 3) and converting it to the base year (2019) using the Chemical Engineering Plant Cost Index (CEPCI) as applicable (Eq. 6) [3,61]. The solar field components and the SRC power cycle were calculated using the cost estimates analysis from SAM and converted to the plant base year using an annual inflation rate of 2.1% [62]. Balance of plant (cost of sub-components) including electrical installations, control and instrumentation, insulation, and fittings, tubes, piping and design, platforms, and material erections has been considered in the BMC analysis of the main plant components. Component costs from known base cost (when cost data are available) are scaled to the current size using Eq. 7 using a scaling factor of 0.6 based on the six-tenth factor rule [57,60].

$$\text{New Cost} = \text{Present cost} \ \frac{\text{New CEPCI Index}}{\text{Present CEPCI Index}} \tag{6}$$

$$\text{New equipment cost} = \text{Base equipment cost} \ \left(\frac{\text{New equipment size}}{\text{Base equipment size}}\right)^{0.6} \tag{7}$$

Operating costs were determined based on the cost incurred in running the plant as obtained from the materials and energy balance of all process streams including recurrent cost incurred over the plant life. Table 4 summarises the variable and the fixed operating cost assumptions. The cost of raw materials (ceria, water) was obtained from previous studies [31] while the cost of on-site nitrogen generation was based on industrial consultation and gas price review [63,64].

Table 3. Bare module factor of various component of the syngas fuel plant [3,56]

| Description | Parameter | Bare module factor (BMF) |
|---|---|---|
| Equipment item | Reactors | 3.17 |
| | Heat exchangers, recuperators, generators | 3.17 |
| | Splitters | 2.03 |
| | Mixers, cyclone | 2.03 |
| | Heliostat field and towers | 1.25 |
| | Furnaces and direct fired heaters | 2.19 |
| | Parabolic dish collector, volumetric receiver | 1.25 |
| | PTC solar field and receiver, power blocks | 1.25 |
| Process machinery | Pumps, filters, seal | 3.30 |
| | Storage | 1.83 |

### 3.2 Minimum selling price and levelized cost

The minimum selling price (MSP) is the price at which the product must be sold for such that the NPV is equal to zero at the end of the project. Since the DPP is the break-even point whereby the plant's discounted cash flows are equal to its overall cost, the given market price of the plant's products at this point is the MSP [3,65]. The DPP for the TCWS plant is expressed as a function of the DCF:

$$\sum_{n=0}^{DPP} DCF_n = 0 \ |years| \tag{8}$$

$$DCF_n = \frac{CF_T}{(1+d)^n} \tag{9}$$

The DCF is given by cash flow after tax ($CF_T$) based on the discount rate (d) for the nth plant operational years. The discounted cash flow analysis was used to calculate the net present value (NPV) and internal rate of return (IRR). Interest towards loan repayment was not considered in this analysis for consistency.

The levelized cost of hydrogen (LCOH) is expressed in Eq. 10-11, which is similar in approach to the levelized cost of energy (LCOE) for renewable energy generation plants [66].

$$\text{Levelized cost of } H_{2(N)} = \frac{\text{CAPEXxCRF} + [\text{OPEX(fixed,variable)} - \text{Carbon emission tax} - \text{revenue from other products}]}{\text{Annual } H_2 \text{ production (kg)}} \quad (10)$$

Where CAPEX is the total capital investment ($C_{TCI,n}$), OPEX is the total operational cost $C_{op,n}$ (fixed and variable), annual hydrogen fuel production in the plant in kg for the nth plant operational life is taken for 30 years. The annual operational period is assumed at 350 days/y for the TCWS plant. CRF is the capital recovery factor which is given by:

$$CRF = \frac{(1+d)^n * d}{(1+d)^n - 1} \quad (11)$$

The discount rate is a reflection of the level of risk and expected reward an investor is willing to undertake with a higher discount rate showing a higher investment risk [65,67]. The discount rate used for the MSP calculation was 12% which is consistent with process engineering plant economic assessment as against the 5% applicable with renewable energy or solar-based generation plants [60]. As noted in the study of Onigbajumo et al. [3], a discount rate consistent with process engineering-based economic assessment is recommended for solar or renewable energy-driven process plants for LCOE or MSP estimation. This was to avoid distortion of the NPV at the end of the plant project caused by using LCOE calculations with a discount rate suitable to renewable electricity generation. The revenue estimates of the product gases (hydrogen and oxygen) in this work are factored in using prices from previous studies [3,60,68] while the electricity price of the solar field power cycle is estimated using the 2019 electricity industrial purchase price [60]. The discount rate for levelized cost is consistent with relevant literature [69,70], see Table 4.

Table 4. Economic model considerations

| Parameter | Value | Unit* | Ref |
|---|---|---|---|
| Ceria particle fluidization | 80000 | kg/h | |
| Operation period | 350 | d/y | |
| Minimum solar active period** | 8 | h | |
| Maximum non-solar period of the year | 20 | d/y | |
| Total electricity generation sold to the grid | 103 | MWh/y | |
| Electricity consumed for plant process | 24.5 | MWh/y | |
| [a]Ceria particle feed replacement | 5 | cycles/y | [71] |
| Operational plant life | 25 | y | |
| Fluidized bed reactor | 2400 | USD/m$^2$ | [31,58] |
| Reactor material type | Inconel 625 | | [60] |
| Recuperators and heat exchangers | 3600 | USD/m$^2$ | [58] |
| Pressure Pumps | 1600 | USD/kWh | [57,58] |
| Cyclone | 6484 | USD/m$^3$ | [57,58] |
| Vacuum pumps | 2242 | USD/m$^3$ | [57,58] |
| [b]Separator | 173,022 | USD/m | [57,58] |
| Mixer | 230 | USD/m$^3$ | [57,58] |
| Factor of material | 1.2 | | [31] |
| Gas storage period | 24 | h | |
| <u>Economic consideration</u> | | | |
| Capacity factor | 0.7 | | [61] |
| [c]Location factor | 1.4 | | [3,61] |
| Annual inflation rate | 1.7 | | [62] |
| CEPCI for study year (2019) | 607.5 | | [72] |
| CEPCI 2002 annual average | 390.4 | | [57] |
| CEPCI 2014 annual average | 576.1 | | [58,73] |
| CEPCI 2015 annual average | 556.8 | | [31,72] |
| Exchange rate (2015) | 0.7981 | USD/AUD | [62] |
| Exchange rate (2016) | 0.7287 | USD/AUD | [3,62] |
| Exchange rate (2019) | 0.7268 | USD/AUD | [3,62] |
| Ceria particle cost | 7.4 | USD/kg | [31] |
| Cost of nitrogen | 0.16 | USD/m$^3$ | [63,64] |
| Price of oxygen | 0.07 | USD/kg | [68,74] |
| Cost of water | 2 | USD/m$^3$ | [60] |
| Price of electricity | 38.95 | USD/MWh | [31,75] |

| | | | |
|---|---|---|---|
| Operators | 1 per 1-10 | t/h | [3,60] |
| Carbon tax ($CO_2$ emission) | 17.69 | USD/ton | [60,76] |
| Annual wages | 105,000 | USD/operator | [3] |
| Insurance and taxes | 1.5 | % $C_{TCI}$ | [3,56] |
| Operations and maintenance | 1.5 | % $C_{TCI}$ | [3,61] |
| Discount rate (LCOH analysis) | 5 | % | [70] |
| Discount rate (DCF and NPV analysis) | 10 | % | [31,61] |
| Solar field[d] (SAM Modelling) | | | |
| DNI[e] | 950 | W/m² | |
| Total land area | 24282 | m² | |
| Solar concentration ratio | 1 | kW/m² | [43] |
| Solar multiple | 3.5 | | [3,43] |
| Efficiency of concentrator | 80 | % | [43] |
| Efficiency of receiver | 70 | % | [43] |
| Contingency cost | 7 | % | |
| EPC | 13 | % TDC[f] | |
| Land cost (% of direct cost) | 2 | % | |
| Steam Rankine power cycle | | | |
| Site improvement | 16.3 | USD/m² | |
| SRC design cost | 700 | USD/kWe | |
| Balance of plant cost | 220 | USD/kWe | |
| Sales tax (on 80% direct cost) | 5 | % | |
| PDC and solar receiver | | | |
| Site improvement | 20.3 | USD/m² | |
| Collector cost | 270 | USD/m² | |
| Receiver cost | 185 | USD/m² | |
| PV-battery system | | | |
| Module cost | 0.2 | USD/Wdc | |
| Inverter | 0.7 | USD/Wdc | |
| Battery pack | 150 | USD/kWh dc | |
| Battery power | 300 | USD/kWh dc | |
| Balance of system | 0.15 | USD/Wdc | |
| Site improvement cost | 0.03 direct cap. cost | | |

*All cost and pricing are in 2019 USD.

** Minimum solar active period was considered to reduce the chance of underestimation. Solar active period for the proposed plant location is able to reach 12 hours per day (see supplementary material).

[a] Ceria particle is assumed to be stable over 2000 cycles according to Rhodes et al. [71], 1500 cycles was considered for the economic consideration.

[b] Separator design for economic estimation is based on the bowl diameter of the reactor.

[c]Location factor was based on the plant site in Australia.

[d] Energy estimate and size of solar field was calculated based on the approximate energy results using Aspen Plus modelling. Solar field design and cost estimation was performed using NREL SAM (Version 2018.11.11)

[e] Average DNI obtainable using data available from Australian Government Bureau of Meteorology for Northern Queensland [77].

[f] Total direct cost of solar field design

### 3.3 Sensitivity and switch value analysis

The key variables which affect the MSP and economic potential of the TCWS are split into CAPEX and OPEX regime for sensitivity analysis by ±25% in both directions of the base value of the component. Sensitivity analysis for the capital cost-based variables includes solar field, tax and insurance, reactor, heat exchanger, and discount rate. The operating cost-based variables include the cost of ceria particle, $N_2$ gas supply, price of $H_2$ and $O_2$ gas sales, and the price of electricity. The parameters with a significant impact on the economic potential of the TCWS process are analysed and discussed in the next section.

The switch value analysis provides an understanding of the percentage deviation or change with which a variable affecting the MSP must be varied to achieve a zero NPV. This helps to eliminate possible bend that is not covered with the use of sensitivity analysis [67]. According to Onigbajumo et al. [3], switch value (SV) is given by:

$$SV = \frac{(100 \times NPV_b)\,(X_b - X_n)}{(NPV_b + NPV_n)\,X_b} \quad (11)$$

Where $NPV_b$ and $X_b$ are the NPV and the base case value of parameter *X*, $NPV_n$ and $X_n$ are the net present value and the change values of parameter X at the new point "n" to achieve the net present value of zero.

## 4. Results and discussion

### 4.1 Process model

Presented in Table 5 are the results of the material and energy balance of the TCWS process model on the basis of 1kg per hour of hydrogen gas produced from the thermochemical reduction of 80 t/h of ceria particles. Overall energy consumption included 36.4 MW for thermochemical reduction and 8.3 MWe to drive electrical components such as pumps and control systems. The TCWS plant produced 461 kg/h hydrogen, 3712 kg/h oxygen, and 18.9 MWh of electricity from the SRC power block which can be sold to augment non-solar hour operations and overall production cost. The process was mostly self-sustained in terms of materials and energy requirements. For instance, ceria particles were recycled or re-used for an average of 1500 recycles (taking a recycle as an hourly operation) which brings the total ceria particle feed replacement to approximately 5 cycles/y. Nitrogen gas was completely recycled and not consumed in the reduction reaction in the FBRR unit, however, the plant for economic consideration assumed nitrogen gas was purged once every 30 days. Only 13.5% of the 29.3 t/h water requirement by the plant was consumed while 50.11% of the energy nameplate of the TCWS plant was recovered in net electricity production in the SRC power cycle with 36.88 MW steam recovery.

Table 5. Mass and energy balance from the TCWS process model

| Stream | Production (per kg $H_2$ per hour) | Units |
|---|---|---|
| **Ceria (inlet)** | 173.54 | kg |
| **Water (inlet)** | 31.39 | kg |
| **$H_2$ (product)** | 461 | kg |
| **$O_2$ (product)** | 8.1 | kg |
| **Steam (to SRC)** | 22.34 | kg |
| **$N_2$ gas (recycled)** | 3.25 | kg |
| **Ceria (recycled)** | 173.42 | kg |
| **Solar field and volumetric receiver** | 0.1375 | MWh |
| **TCWS (FBRR and FBOR)** | 0.11 | MWh |
| **PV electricity (pumps and control systems)** | 0.018 | MWh |
| **Stored energy (hydrogen, steam)** | 0.045 | MWh |
| **Sensible heat in gaseous products (hydrogen, oxygen)** | 0.081 | MWh |
| **SRC electricity (power block)** | 0.041 | MWh |
| **Energy losses** | 0.016 | MWh |

The accuracy of the TCWS process model was compared with the experimental works of Taghipour et al. [81] for the fluidization velocity and drag velocity of the indirectly irradiated ceria particle through nitrogen heating. The simulated bed pressure drop and instantaneous voidage fraction with the local voidage profiles of the experimented results of Taghipour et al. [81] at particle diameter of 275 μm at a fluidization velocity of $U_{mf}$ = 0.38 and 0.46 m/s at a height z = 0.2 m were closely matched. (See supplementary material).

### 4.2 Economic model

The capital cost estimation is based on the bare module cost approach of Seider et al., [55] and the author's previous work [3] which accommodates equipment inflation as part of the approach. However, currency conversion is not included explicitly in the method like other approaches too. Table 6 presents the results of the economic evaluation of the TCWS model detailing the capital and operating cost breakdown. The levelized cost of hydrogen was estimated using a similar approach for LCOE assessment based on capital recovery factor and a discount rate of 5%. The MSP for hydrogen was however estimated at a discount rate of 12% based on the discounted cash flow analysis where the NPV of the plant is zero at the end of the plant operational life. The comparison between LCOE at 5% and MSP at 12% discount factor for this study will be discussed in the later section.

Table 6. Capital and operating cost breakdown for the TCWS plant.

| Item | Value in 2019 million USD |
|---|---|
| **Process Plant** | |
| **Heat exchangers, steam generators, and recuperators** | 0.37 |
| **Pressure pumps** | 1.31 |
| **Vacuum pumps** | 2.01 |
| **Control valves** | 0.21 |
| **Mixers** | 0.01 |
| **Separators** | 1.15 |
| **Cyclones** | 0.97 |
| **Reactors (FBRR and FBOR)** | 1.53 |
| **$O_2$ Storage** | 4.75 |
| **$H_2$ storage** | 11.8 |
| **Site Preparation (15% installed cost, including earthworks, piping and installation)** | 3.48 |
| **Service facilities (20% installed cost)** | 4.65 |
| **Direct primary investment (direct cost)** | 31.35 |
| **Total depreciable cost** | 37 |
| **Total permanent investment** | 41.44 |
| **Working capital** | 6.22 |
| **Total capital investment (TCI or CAPEX-plant) of TCWS plant** | 47.65 |
| **Solar Field** | |
| **Engineering procurement and construction** | 2.54 |
| **Site preparation** | 0.75 |
| **Contingency cost** | 1.88 |
| **PDC and solar volumetric receiver** | |
| **Collectors** | 1.65 |
| **Receivers** | 9.32 |
| **Steam Rankine power cycle** | |
| **Design cost (direct cost)** | 20.3 |
| **Balance of plant (indirect cost)** | 6.38 |
| **PV-Battery System** | |
| **Total direct cost (module, inverter, battery, installation, overhead)** | 7.95 |
| **Indirect cost (balance of system equipment)** | 3.74 |
| **Total capital investment (CAPEX-solar)** | 54.16 |
| **Total capital cost of the TCWS and energy system** | 101.81 |
| **Operating cost (OPEX-variable and fixed)** | |
| **Ceria particle** | 2.96 |
| **Water** | 0.067 |
| **Nitrogen (purge once every 30 days)** | 0.031 |
| **Electricity (non-solar hours)** | 6.82 |
| **Wages** | 3.15 |
| **Annual insurance and tax (1% TCI)** | 1.13 |
| **Maintenance (1% TCI)** | 1.13 |

*see previous data in Table 4 for economic considerations and assumptions.

4.2.1 Capital cost of the TCWS plant

The total capital investment (total capital cost) of the TWCS plant and the energy systems was approximately 102 million USD. The process plant contributed 46.8% at 47.7 million USD and the solar field asset including the PDC and solar receiver, PV solar field, and SRC power block contributed 53.2% at 54.16 million USD to the total capital investment. See details of solar field asset capacity in Table 5. The TCI is comparable with the capital cost estimate by Budama et al. [31], however, the current study presents more extensive details and economics of scale for both process and solar field models. Fig. 6 shows the total capital investment breakdown of the plant with each component presented as a multiple of total depreciable cost, permanent investment, and working capital (see Table 3).

The SRC power cycle, hydrogen storage, parabolic dish collectors and solar receivers, PV solar field, and oxygen storage are the highest contributors to the capital cost of the solar-driven TCWS plant at 33.02%, 26.75%,

14.31%, 11.12%, and 9.57%, respectively. Other components of the TCI comparable to previous studies are the vacuum pumps at 4.05% (4.13 million USD) and the reactors at 3.08% (3.13 million USD). Budama et al. [31], Falter and Sizmann [78], and Falter et al. [79] reported similar highest contributions of solar field assets (heliostats, solar tower), vacuum pumps, gas storage, and reactors to the total capital investment. The annualized capital investment at a 5% plant depreciation rate was 6.62 million USD/y, while the capital cost per kg hydrogen production was 0.87 USD/kg $H_2$. Another important part of the analysis is the cost of fluidized bed reactor per kg of hydrogen produced which is 0.0012 USD/kg $H_2$. However, hydrogen storage on-site at 1.6 MPa pressure, as buffer prior to transport to the final consumers is approximately eight times the cost of a fluidization reactor at 0.0089 USD/kg $H_2$. The cost of solar energy installation per kg of hydrogen produced over the plant life is 0.21 USD/kg $H_2$ and the cost of SRC power cycle generation is 0.26 USD/kg $H_2$ produced.

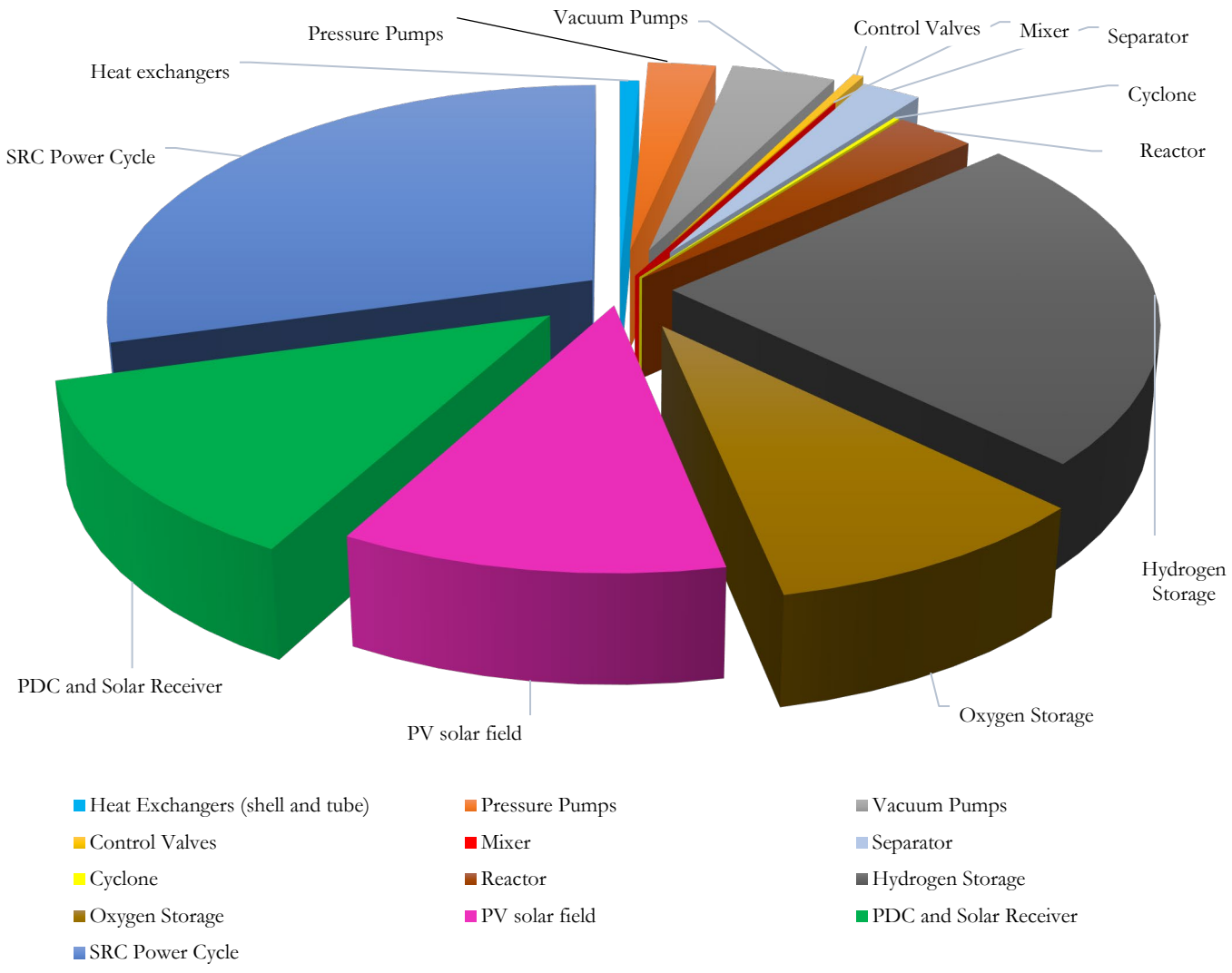


Fig. 6. Total capital investment (Million USD) breakdown for the thermochemical water splitting plant for hydrogen production, water, and electricity cogeneration.

If the cost of solar energy assets such as heliostat, concentrators, receivers, and solar towers were halved based on mid-term future projections of the CST technology maturity [84], the annualized capital cost at 5% depreciation would reduce by 20.24 % (5.28 million USD/y). At this projection, the capital cost per daily hydrogen production was estimated to be 0.7 USD/kg $H_2$. Shorter gas storage periods and higher pumping efficiency are potential options for achieving up to 12-26.8% reduction in total capital investments of the TCWS plant.

### 4.2.2 Operation and maintenance cost of the TCWS plant

The estimated annual operating cost (OPEX) for the TCWS plant was 15.6 million USD (see Fig. 7). The highest contribution to annual OPEX is the cost of electricity consumption for a non-solar operational period at 49.41% (6.82 million USD). If the PV-battery solar field were not integrated into the plant set-up, the contribution of the cost of electricity to annual OPEX would have increased by 22.85% amounting to 56.68% contribution to OPEX at 8.84 million USD. The largest contribution to the operating cost was the electricity consumption on the basis of 16 hours of non-active solar availability (Table 4) for the proposed plant site (see section 2.3). This was considered to be a lower limit of solar utilisation. However, based on the result of hourly, daily, and annual solar DNI modelling of the proposed plant location using the available data from the Australian Government Bureau of Meteorology [77], an estimated projection of a 14-hour non-solar period was considered to be consistent with the average number of solar hours of the plant proposed site. The results of the modelling show that the plant could run on a 14-hours non-solar period for 350 days of solar-driven plant operation for the TCWS.

The next major contributor to the OPEX was the cost of ceria particles which was found to be 21.44% (2.96 million USD). Other major cost contributors were the cost of labour at 13.69% (1.89 million USD) due to the additional electricity co-generation, followed by the cost of insurance and tax, and annual maintenance costs each at 7.37% (1.02 million USD). The operating cost per kg of hydrogen produced in the absence of a PV-based solar field to drive the pumps and other electrical systems of the plant was 4.03 USD/kg $H_2$ with non-solar electricity consumption at 2.28 USD/kg $H_2$. Alternatively, with a PV-based solar field installed in the TCWS plant to reduce electrical consumption costs, the operational cost per kg hydrogen was reduced by ~11% to 3.57 USD/kg $H_2$. The non-solar electricity consumption cost of the TCWS plant at the same time was reduced by 22.8% to 1.76 USD/kg $H_2$ due to solar PV integration. The ceria particle feed was at 0.76 USD/kg $H_2$ while the annual insurance cost was 0.26/kg $H_2$.

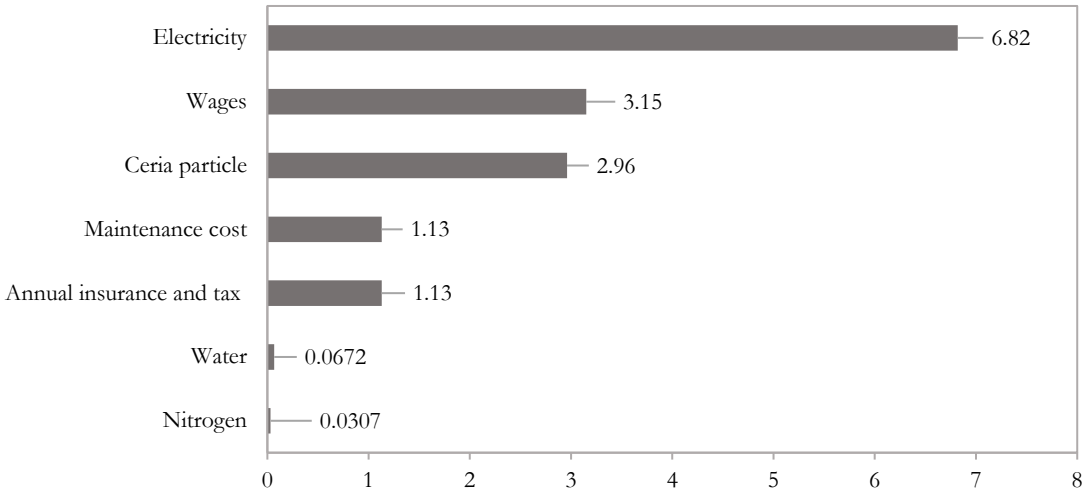


Fig. 7. Operational (fixed and variable) cost breakdown for the thermochemical water splitting plant.

### 4.2.3 Levelized cost and minimum selling price

The levelized cost and minimum selling price of hydrogen were based on USD per kg of $H_2$ produced (2019 basis). While LCOH was estimated at a 5% discount rate consistent with other studies with LCOE calculations for CSP-based plants, the MSP for hydrogen was estimated at a 10% discount rate with regards to process-engineering-based plants cost assessment [3]. The LCOF was estimated as 2.66 USD/kg $H_2$, while the MSP estimation resulted in 3.92 USD/kg $H_2$. The lower selling price achieved in this work is a function of oxygen and electricity co-production in the TCWS hydrogen plant, without which the MSP would have been 4.17 USD/kg $H_2$ (less oxygen revenue) and 4.51 USD/kg $H_2$ (less electricity revenue). If the revenue from oxygen and electricity co-production were absent from the TCWS plant, the MSP of hydrogen would be 6.05 USD/kg $H_2$. Using the MSP as the basis of economic viability and performance of the TCWS plant, the contributions of key plant capital investment and operation cost are presented in Fig. 8.

Power generation with the SRC power block, hydrogen storage, PDC and volumetric solar receiver, PV solar field, and oxygen storage were the highest contributors to minimum selling price at 1.01 USD/kg $H_2$, 0.82 USD/kg $H_2$, 0.44 USD/kg $H_2$, 0.38 USD/kg $H_2$, and 0.33 USD/kg $H_2$, respectively. For the operating cost, non-solar period electricity consumption 0.23 USD/kg $H_2$, ceria particle at 0.1 USD/kg $H_2$, and labour cost at 0.06 USD/kg $H_2$ were the largest contributors to the MSP of hydrogen, respectively. From these analyses, about 47% of the MSP is contributed by solar energy assets and components of the plant configuration alone. This is an indication that future price reduction in the cost of CST materials and installation will have a significant impact on the MSP of hydrogen which may be applicable to other solar-based renewable energy-driven hydrogen production. The integration of PV solar field to drive the electrical energy requirements for pumps, machines and other control systems increased the capital cost by 12.5% from 90.49 million to 101.81 million USD. However, over the operational lifetime of the plant, the PV-solar field was able to reduce energy costs and lowered MSP by 9.5%.

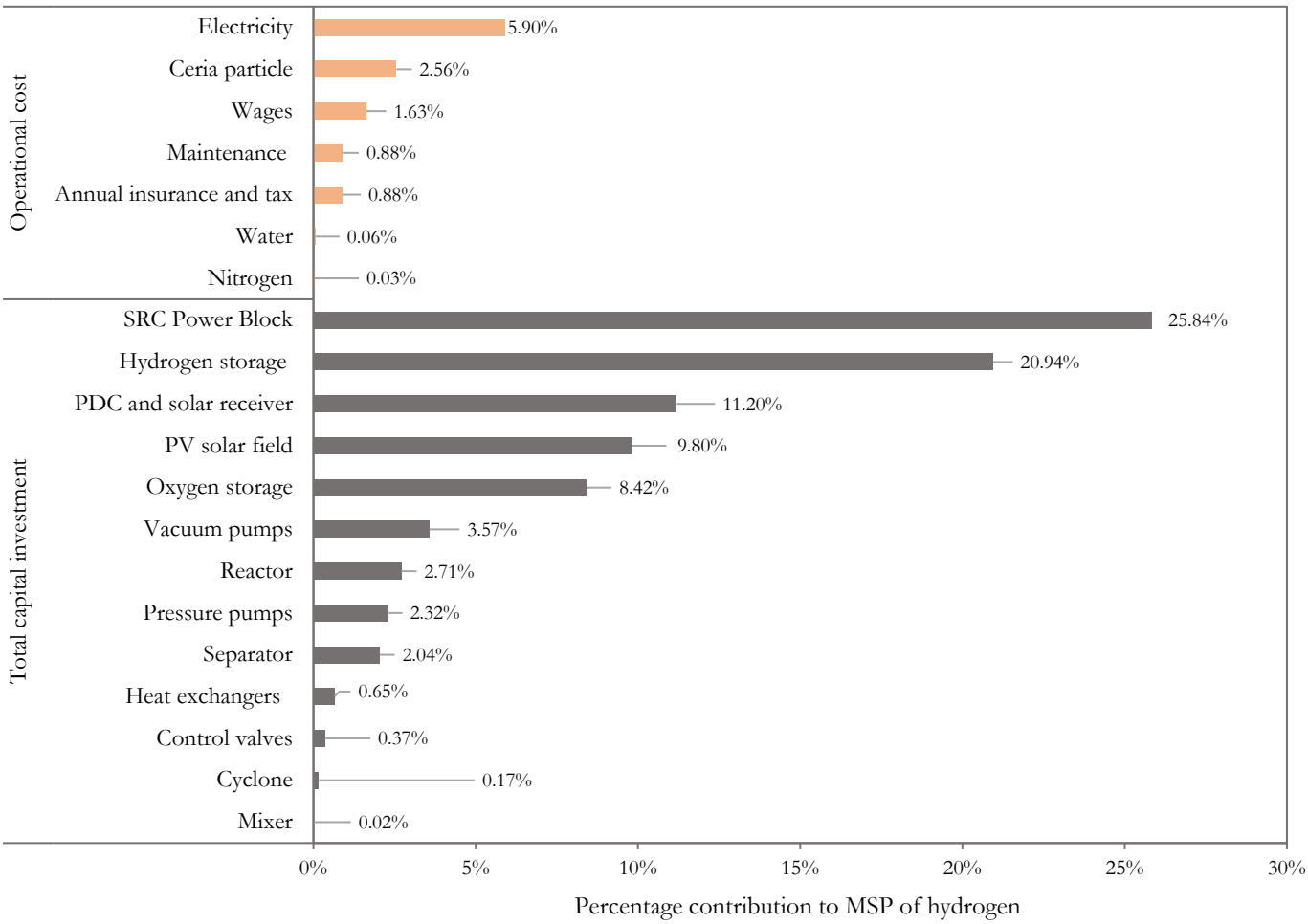


Fig. 8. Percentage contribution of the components of capital investment and operational cost to the minimum selling price of hydrogen.

Table 7 shows the comparison between the minimum selling price obtained in this work with the levelized cost or MSP obtained in other previous studies for the production of hydrogen. Moser et al., [41] reported the highest selling price of 38.83 €/kg $H_2$ (~ 43.49 USD/kg $H_2$ in the year 2019) via thermochemical water splitting of ceria and nickel-ferrite oxides using a heliostat-based solar tower system. The authors expressed optimism of producing hydrogen at 6.68 €/kg $H_2$ (~7.48 USD/kg $H_2$ in year 2019) at 5% discount rate if multiple contributing factors were significantly reduced. Khodabandehloo et al., [80] was the closest study to this work with reference to the costing year and discount rate with their study focused on hydrogen production via steam methane reforming (SMR) and aqueous phase reforming (APR) of glycerol. This approach using electrical energy delivers hydrogen at the lowest of 7.45 USD/kg $H_2$.

Table 7. Comparative summary of the MSP/LCOH of previous studies on hydrogen production with current work.

| Study | Approach | Energy option | Discount rate | Costing year | MSP/ LCOH | Remark |
|---|---|---|---|---|---|---|
| Current study | Thermochemical water splitting of ceria, hydrogen production, oxygen, and electricity co-production | Concentrated solar thermal, PDC and volumetric solar receiver | 10% | 2019 | 3.92 USD/kg $H_2$ | Higher chance of achieving 2 USD/kg $H_2$ with single factor variation |
| Khodabandehloo et al. [79] | Glycerol reforming using steam methane reforming (SMR) and aqueous phase reforming (APR) | Electricity integration | 10% | 2019 | 7.49 USD/kg $H_2$ (SMR) and 7.45 USD/kg $H_2$ (APR) and 7.45 USD/kg $H_2$-APR | 48% probability to achieve 3.55 USD/kg $H_2$ |
| Budama et al. [30] | Thermochemical water splitting of ceria, hydrogen and electricity production, CO co-production | Concentrated solar thermal, heliostat and solar tower receiver | 8% | 2015 | 4.55 USD/kg H2 | Optimistic about achieving 2 USD/kg $H_2$ by varying multiple connected variables |
| Moser et al., [40] | Thermochemical water splitting of ceria and nickel-ferrite oxides | Concentrated solar thermal, heliostat and solar tower receiver | 5% | 2015 | 38.83 €/kg H2 (nickel-ferrite) 13.06 €/kg $H_2$ | Optimistic that selling price could reduce to 6.68 €/kg H2 |
| Kim et al., [80] | Methane reforming for hydrogen production with membrane reactor (MR) and packed bed reactor (PBR) | Electricity | 2-10% | 2015 | 6.48 USD /kg $H_2$ (MR), 11.18 USD/kg $H_2$ (PBR) | Optimistic value not indicated |

Budama et al. [31] however produced hydrogen via thermochemical water splitting as presented in this work but with a similar CST energy integration approach as Moser et al., [41] at a 8% discount rate to achieve a minimum selling price of 4.55 USD/kg $H_2$. This work is novel by delivering an improved hydrogen production per MW of energy input using solar irradiated nitrogen for ceria particle heating compared to Budama et al. [31] who had proposed that solar-driven TCWS with ceria is not economic. The TCWS plant proposed in this study is economic at 3688 kg/day per 50.71 MWth PDC assembly (considering active solar hours alone) when compared with 1431 kg/day per 27.74 MWth heliostat-based solar tower from the comparative work [31]. At the comparative discount of 8% in other studies, this work produced hydrogen at 3.47 USD/kg $H_2$ which is ~24% lower than the price in Budama et al. [31].

It is important to note that effort to reduce the impact and trend of global climate change has continued to positively affect the utilisation of hydrogen as the future fuel. To achieve meaningful penetration and utilisation at a larger scale, declining costs are key, especially for green hydrogen (zero carbon emission during production). More nations have continued to set goals and targets for their hydrogen production plan capable of making the price very attractive and competitive. The United States Department of Energy (D.O.E) had recently unveiled the plans and initiatives (Hydrogen Shot) to reduce energy bottlenecks and cost by 80% to bring hydrogen selling price to 2 USD/kg $H_2$ from the current cost estimate of 5 USD/kg $H_2$ [81]. Southern Europe is targeting a renewable hydrogen cost target of 1.5 €/kg $H_2$ by 2030 [82]. In Australia and Asia, policies and plans are designed to also achieve 2 USD/kg $H_2$ before 2050 [83].

Notwithstanding, to realise the target of 2 USD/kg $H_2$ as proposed by Budama et al. [31] will require that multiple variables such as the cost of solar field assets, reactors, receivers, the balance of plant, and recovery factor are reduced to a considerable degree at the same time while increasing the solar field efficiency and electricity sales price. Fig. 9 shows a comparison of the MSP obtained in this work with previous studies based on the discount rate used (all prices are in the year 2019). The current work has shown better performance for a lower MSP and had a higher potential of realising the target price of hydrogen at a global scale compared to all the studies assessed. The

economic indicators to achieve the target hydrogen price of 2 USD/kg $H_2$ according to the US D.O.E and other global policy goals are discussed in the next section.

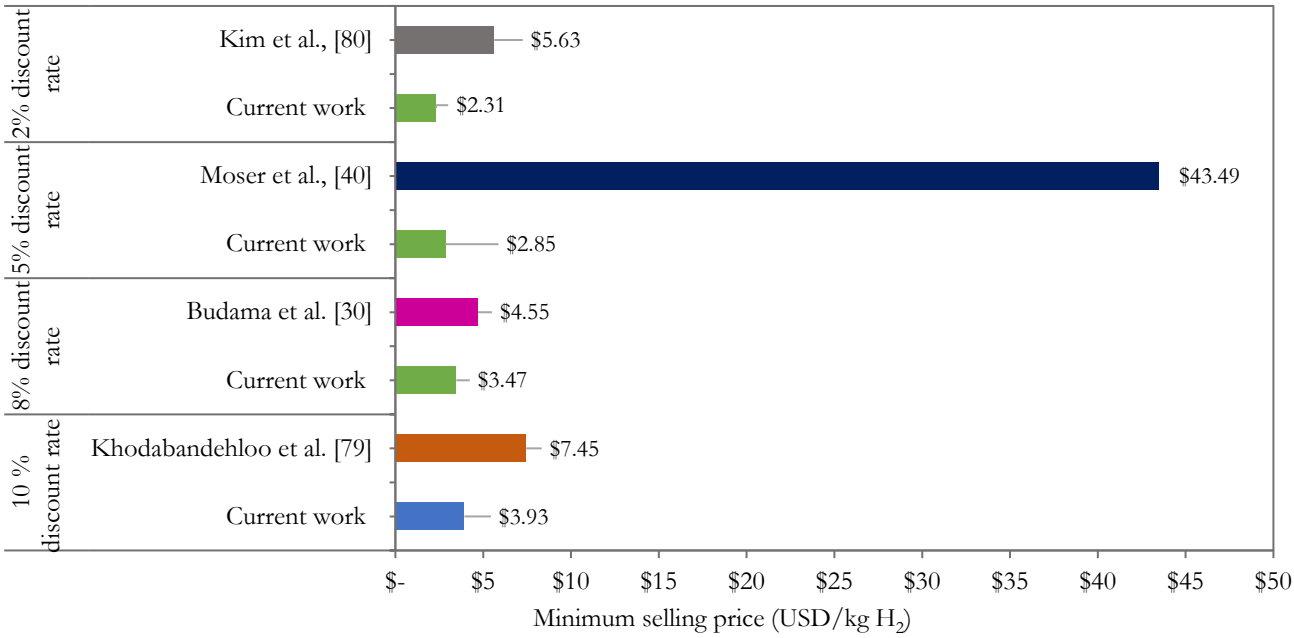


Fig. 9. Comparison between the minimum selling price in current work and previous studies based on discount rate.

4.2.4 Sensitivity and switch value analysis

The sensitivity analysis (Fig. 10) was performed to consider the economic viability of the TCWS process in this study considering potential future possibilities and sustainability. The sensitivities of parameters with the highest contributions to the minimum selling price are provided in the figure.

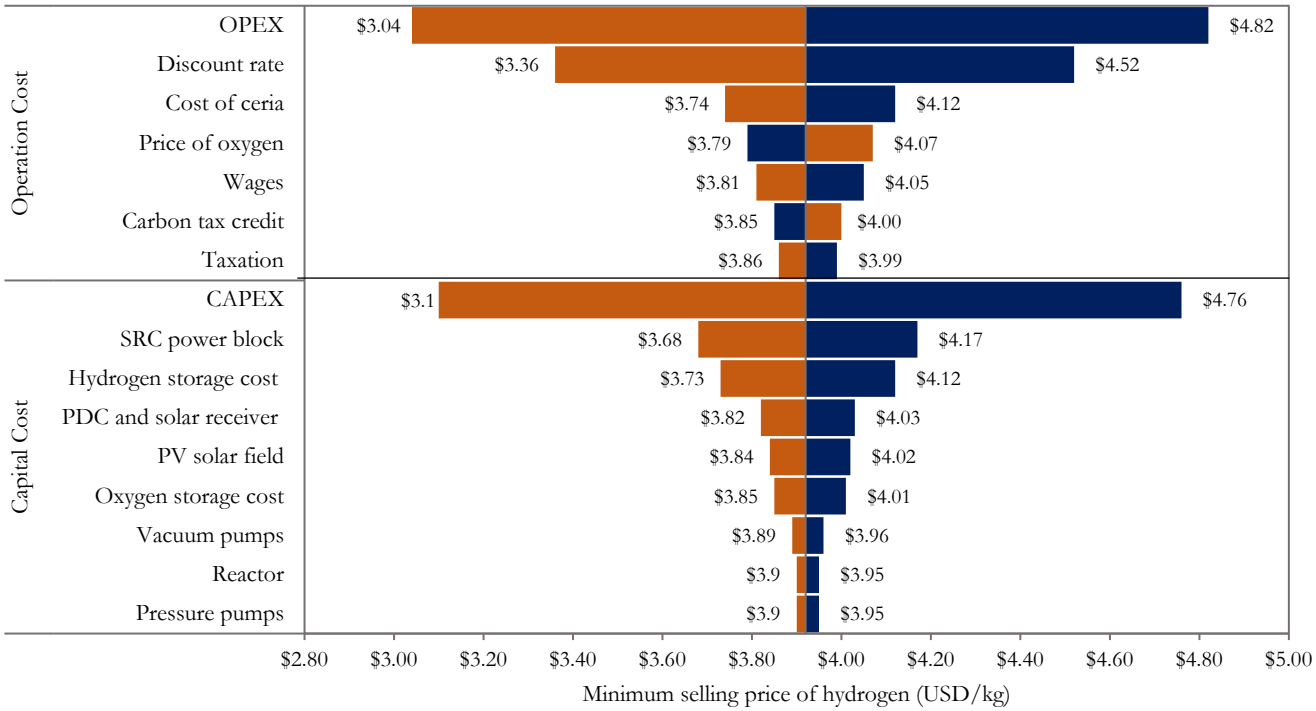


Fig. 10. Sensitivity analysis of the minimum selling price of hydrogen for the TCWS plant.

A 25% reduction in both OPEX and CAPEX had the most significant effect on the MSP of hydrogen at 22.4% (3.04 USD/kg $H_2$) and 21% (3.1 USD/kg $H_2$), respectively. For OPEX, the discount rate was particularly important at 25% lower (7.5 % discount rate) leading to a 14.3% reduction in MSP to 3.36 USD/kg $H_2$ which is still higher than the discount factor implicit in LCOE (i.e., 5%). With reference to the levelized cost of hydrogen from the study of Budama et al. [30], most of the variables considered in this work (with exception of CAPEX and OPEX) are able to achieve MSP of hydrogen for less than 4.55 USD/kg $H_2$ even at 25% increase in future price. An important factor in the reduction of the MSP is the option of PV-battery module solar field integration which reduced the MSP of hydrogen for the TCWS plant by ~10% from 4.31 USD/kg $H_2$ (if grid electricity was utilised for machinery and control systems) to 3.92 USD/kg $H_2$. Hence, the cost of electrical energy usage even at a 25% cost reduction still resulted in the MSP of hydrogen at 4.07 USD/kg $H_2$.

The sensitivity analysis showed some parameters had more effect on the economic performance of the TCWS compared to others. The switch value analysis was therefore assessed based on the percentage change in the cost of single key parameters that has the most significant effect on the TCWS plant to achieve the future hydrogen target price of 2 USD/kg $H_2$ [81,83]. Table 8 shows the switch values which the TCWS plant is economic for the selected parameters with reference to three discount rate regimes. At a 10% discount rate, none of the parameters had their switch values below 50% reduction. At 8% and 5% discount rates, however, a 41.5% and 23.7% reduction in OPEX, respectively, would deliver hydrogen price at 2 USD/kg $H_2$.

Table 8. Switch value analysis for the most significant parameters of economic viability of the TCWS plant at 10%, 8%, and 5% discount rate to achieve 2 USD/kg $H_2$.

| **Discount rate** | **10%** | **8%** | **5%** |
|---|---|---|---|
| **Parameter** | | **Switch Values** | |
| Annual OPEX | [<]* $6,351,016 | [<] $8,076,835 | [<] $10,534,402 |
| Annualized CAPEX | [<] $42,761,142 | [<] $49,378,938 | [<] $ 63,123,590 |
| Price of oxygen | [>] $ 0.31 USD/kg | [>] $0.25 USD/kg | [>] $0.17 USD/kg |
| Process yield | [>] 1.96 | [>]1.74 | [>] 1.42 |
| Carbon tax credit | [>] 130 USD/tonne | [>] 103.5 USD/tonne | [>] 67.2 USD/tonne |

*indicates the direction which determines whether an increase [>] or decrease [<] of the parameter in the switch analysis will yield a zero NPV.

A 38% reduction in CAPEX with a 5% discount rate would be required to achieve the target price of hydrogen (2 USD/kg $H_2$). If oxygen were sold at 0.31 USD/kg, the TCWS plant proposed in this study would be economic and hydrogen could be sold at the future target price even at 10% discount rate. At a lower discount rate of 5%, oxygen could be sold even for 0.17 USD/kg while maintaining the economic viability of production at future hydrogen price. Although switch value analysis is useful to show economic potential with a single component reduction, it is more realistic to use a multi-component approach to reduce the selling price while assessing economic viability with future changes. For instance, a 22% reduction in OPEX, carbon tax credit at 71 USD/ton, and oxygen sold at 0.14 USD/kg simultaneously bring the plant to achieve the future hydrogen price. A higher carbon tax credit at about six times the current rebate can be applied with all other parameters constant to make the plant economic at 8% discount rate which is a promising future economic possibility. Also, in recent times, the oxygen spot market price has been volatile due to the COVID-19 pandemic, as such, the price of oxygen has ranged between 0.32-0.49 USD/kg (prices were regressed to 2019) [88]. Taking the average oxygen price of 0.4 USD/kg, hydrogen could be sold for 1.26 USD/kg $H_2$ without simultaneous reduction in other components of CAPEX and OPEX, including the discount rate. If oxygen is sold at 0.32 USD/kg at a 5% discount rate, hydrogen can be sold for as low as 0.83 USD/kg $H_2$. It is important to note that the lower prices of hydrogen in this work are achievable due to the revenue obtained from oxygen and electricity as co-products of the TCWS plant.

## 5.0 Conclusion

This work presented a novel approach for solar thermochemical hydrogen production using indirectly solar irradiated ceria and assessed the economic performance of the commercial-scale plant to produce hydrogen at 461 kg/h. An important outcome of the TCWS process modelling using the fluidized bed reactor is the effect of nitrogen gas flow rate on the hydrogen gas yield. It was found that hydrogen gas yield could be improved without considerable change in the non-stoichiometric oxygen yield when nitrogen gas flow rate increases over a maximum which no further effect was observed. The economic performance of the TCWS plant resulted in the production of hydrogen with the co-production of oxygen and electricity at 3.92 USD/kg $H_2$ at a 10% discount rate consistent with the process-engineering-based plant. However, when compared with other studies where lower discount rates were used, the TCWS modelled in this study has the potential to produce hydrogen at 2.85 USD/kg $H_2$ at a 5% discount rate. A key advantage of the indirectly irradiated ceria reduction approach used in this work that impacted the overall plant economics was the integration of parabolic dish collectors at a modular scale to heat up nitrogen. This lowered the cost of ceria thermo-reduction compared to direct ceria reduction by integrating a heliostat-based solar tower CST, thereby reducing the cost of CST heating on a larger plant scale.

Compared to a similar study where the heliostat solar field contributed 35.2% to the total capital investment, the PDC solar field was shown to contribute less than 13% of the CAPEX in this study, thereby accounting for only 11.2% contribution to the hydrogen selling price. The TCWS hydrogen plant explained in this work was economic at 3688 kg/day hydrogen per 50.71 MWth (yield to energy consumption ratio) with a solar PDC integration when compared with 1431 kg/day per 27.74 MWth heliostat-based solar tower from the comparative work [31]. This solar energy integration approach defines the contribution of this work and provides a pathway for renewable hydrogen fuel via TCWS with ceria as the active material. Achieving the target global hydrogen price of 2 USD/kg $H_2$ based on the results of this study could potentially be realised with a 35% reduction in the operational cost through lower cost of ceria, discount rate, and higher carbon tax credit. Selling the oxygen generated from the TCWS plant at 0.31 USD/kg consistent the with current oxygen market price or a carbon tax credit at 0.13 USD/kg emission could make hydrogen sell at 1.26 USD/kg even at a 10% discount rate. Other opportunities to lower the hydrogen selling price in future works are through shorter residence time for ceria thermo-reduction, and higher economies of scale of the plant. Further recommendations for energy integration in future works is to consider hybrid energy utilisation such as natural gas, electricity, and solar energy combination to drive the TCWS process.


## Acknowledgement

The first author acknowledges the support of Queensland University of Technology under the Queensland University of Technology Postgraduate Research Award (QUTPRA) scholarship.


## References


[1] Arifin D, Ambrosini A, Wilson SA, Mandal B, Muhich CL, Weimer AW. Investigation of Zr, Gd/Zr, and Pr/Zr--doped ceria for the redox splitting of water. Int J Hydrogen Energy 2020;45:160–74.

[2] Farooqui A, Bose A, Ferrero D, Llorca J, Santarelli M. Simulation of two-step redox recycling of non-stoichiometric ceria with thermochemical dissociation of CO2/H2O in moving bed reactors--Part II: Techno-economic analysis and integration with 100 MW oxyfuel power plant with carbon capture. Chem Eng Sci 2019;205:358–73.

[3] Onigbajumo A, Taghipour A, Ramirez J, Will G, Ong T-C, Couperthwaite S, et al. Techno-economic assessment of solar thermal and alternative energy integration in supercritical water gasification of microalgae. Energy Convers Manag n.d.;230:113807.

[4] Waisman H, de Coninck HC, Rogelj J. Key technological enablers for ambitious climate goalsInsights from the IPCC Special Report on Global Warming of 1.5 C 2019.

[5] Adetunji O, Seidu SO. Simulation and Techno-Economic Performance of a Novel Charge Calculation and Melt Optimization Planning Model for Steel Making. J Miner Mater Charact Eng 2020;8:277–300.

[6] Han D, Jiaqiang E, Deng Y, Chen J, Leng E, Liao G, et al. A review of studies using hydrocarbon adsorption material for reducing hydrocarbon emissions from cold start of gasoline engine. Renew Sustain Energy Rev 2021;135:110079.

[7] Safari F, Dincer I. A review and comparative evaluation of thermochemical water splitting cycles for

hydrogen production. Energy Convers Manag 2020;205:112182.

[8] Ehrhart BD, Muhich CL, Al-Shankiti I, Weimer AW. System efficiency for two-step metal oxide solar thermochemical hydrogen production--Part 1: Thermodynamic model and impact of oxidation kinetics. Int J Hydrogen Energy 2016;41:19881–93.

[9] Ball M, Weeda M. The hydrogen economy--vision or reality? Int J Hydrogen Energy 2015;40:7903–19.

[10] Winter C-J. Hydrogen energy—Abundant, efficient, clean: A debate over the energy-system-of-change. Int J Hydrogen Energy 2009;34:S1--S52.

[11] Council H. Hydrogen scaling up: A sustainable pathway for the global energy transition 2017.

[12] Birol F. The Future of Hydrogen: Seizing Today's Opportunities. Rep Prep by IEA G20, 82-83, Japan 2019.

[13] Xiao L, Wu S-Y, Li Y-R. Advances in solar hydrogen production via two-step water-splitting thermochemical cycles based on metal redox reactions. Renew Energy 2012;41:1–12.

[14] Hannan MA, Azidin FA, Mohamed A. Hybrid electric vehicles and their challenges: A review. Renew Sustain Energy Rev 2014;29:135–50.

[15] Jacobsson S, Johnson A. The diffusion of renewable energy technology: an analytical framework and key issues for research. Energy Policy 2000;28:625–40.

[16] Budama VK, Johnson NG, McDaniel A, Ermanoski I, Stechel EB. Thermodynamic development and design of a concentrating solar thermochemical water-splitting process for co-production of hydrogen and electricity. Int J Hydrogen Energy 2018;43:17574–87.

[17] Dincer I, Acar C. Review and evaluation of hydrogen production methods for better sustainability. Int J Hydrogen Energy 2015;40:11094–111.

[18] Dincer I, Zamfirescu C. Sustainable hydrogen production options and the role of IAHE. Int J Hydrogen Energy 2012;37:16266–86.

[19] Mao Y, Gao Y, Dong W, Wu H, Song Z, Zhao X, et al. Hydrogen production via a two-step water splitting thermochemical cycle based on metal oxide--A review. Appl Energy 2020;267:114860.

[20] Alioshin Y, Kohn M, Rothschild A, Karni J. High temperature electrolysis of CO2 for fuel production. J Electrochem Soc 2015;163:F79.

[21] Funk JE, Reinstrom RM. Energy requirements in production of hydrogen from water. Ind \& Eng Chem Process Des Dev 1966;5:336–42.

[22] Nakamura T. Hydrogen production from water utilizing solar heat at high temperatures. Sol Energy 1977;19:467–75.

[23] Steinfeld A. Solar hydrogen production via a two-step water-splitting thermochemical cycle based on Zn/ZnO redox reactions. Int J Hydrogen Energy 2002;27:611–9.

[24] Koepf E, Villasmil W, Meier A. Pilot-scale solar reactor operation and characterization for fuel production via the Zn/ZnO thermochemical cycle. Appl Energy 2016;165:1004–23.

[25] Furler P, Scheffe J, Gorbar M, Moes L, Vogt U, Steinfeld A. Solar thermochemical CO2 splitting utilizing a reticulated porous ceria redox system. Energy \& Fuels 2012;26:7051–9.

[26] Nair MM, Abanades S. Tailoring hybrid nonstoichiometric ceria redox cycle for combined solar methane reforming and thermochemical conversion of H2O/CO2. Energy \& Fuels 2016;30:6050–8.

[27] Lu Y, Zhu L, Agrafiotis C, Vieten J, Roeb M, Sattler C. Solar fuels production: two-step thermochemical cycles with cerium-based oxides. Prog Energy Combust Sci 2019;75:100785.

[28] Ermanoski I, Siegel NP, Stechel EB. A new reactor concept for efficient solar-thermochemical fuel production. J Sol Energy Eng 2013;135.

[29] Ehrhart BD, Muhich CL, Al-Shankiti I, Weimer AW. System efficiency for two-step metal oxide solar thermochemical hydrogen production--Part 2: Impact of gas heat recuperation and separation temperatures. Int J Hydrogen Energy 2016;41:19894–903.

[30] Barcellos DR, Sanders MD, Tong J, McDaniel AH, O'Hayre RP. BaCe 0.25 Mn 0.75 O 3- $δ$—a promising perovskite-type oxide for solar thermochemical hydrogen production. Energy \& Environ Sci 2018;11:3256–65.

[31] Budama VK, Johnson NG, Ermanoski I, Stechel EB. Techno-economic analysis of thermochemical water-splitting system for Co-production of hydrogen and electricity. Int J Hydrogen Energy 2021;46:1656–70.

[32] Kaneko H, Taku S, Tamaura Y. Reduction reactivity of CeO2--ZrO2 oxide under high O2 partial pressure in two-step water splitting process. Sol Energy 2011;85:2321–30.

[33] Bhosale RR, AlMomani F. Hydrogen production via solar driven thermochemical cerium oxide--cerium sulfate water splitting cycle. Int J Hydrogen Energy 2020;45:10381–90.

[34] Arenova A, Kodama S, Sekiguchi H. Biomass pyrolysis in Sn-Bi molten metal for synthesis gas production. J Anal Appl Pyrolysis 2019;137:61–9.

[35] Luciani G, Landi G, Di Benedetto A. Syngas Production Through H2O/CO2 Thermochemical Splitting Over Doped Ceria-Zirconia Materials. Front Energy Res 2020;8:204.

[36] Abanades S, Legal A, Cordier A, Peraudeau G, Flamant G, Julbe A. Investigation of reactive cerium-based oxides for H 2 production by thermochemical two-step water-splitting. J Mater Sci 2010;45:4163–73.

[37] Abanades S, Charvin P, Lemont F, Flamant G. Novel two-step SnO2/SnO water-splitting cycle for solar thermochemical production of hydrogen. Int J Hydrogen Energy 2008;33:6021–30.

[38] Abanades S, Flamant G. Thermochemical hydrogen production from a two-step solar-driven water-splitting cycle based on cerium oxides. Sol Energy 2006;80:1611–23.

[39] Norman JH, Besenbruch GE, Brown LC, O'keefe DR, Allen CL. Thermochemical water-splitting cycle, bench-scale investigations, and process engineering. Final report, February 1977-December 31, 1981. 1982.

[40] Charvin P, Abanades S, Flamant G, Lemort F. Two-step water splitting thermochemical cycle based on iron oxide redox pair for solar hydrogen production. Energy 2007;32:1124–33.

[41] Moser M, Pecchi M, Fend T. Techno-economic assessment of solar hydrogen production by means of thermo-chemical cycles. Energies 2019;12:352.

[42] Restrepo JC, Luis Izidoro D, Milena Lozano Násner A, José Venturini O, Eduardo Silva Lora E. Techno-economical evaluation of renewable hydrogen production through concentrated solar energy. Energy Convers Manag 2022;258:115372. https://doi.org/https://doi.org/10.1016/j.enconman.2022.115372.

[43] Wei B, Fakhrai R, Saadatfar B. The thermodynamic analysis of two-step conversions of CO2/H2O for syngas production by ceria. Int J Hydrogen Energy 2014;39:12353–60.

[44] Islam MT, Huda N, Abdullah AB, Saidur R. A comprehensive review of state-of-the-art concentrating solar power (CSP) technologies: Current status and research trends. Renew Sustain Energy Rev 2018;91:987–1018.

[45] Reddy KS, Nataraj S. Thermal analysis of porous volumetric receivers of concentrated solar dish and tower systems. Renew Energy 2019;132:786–97.

[46] Puig-Gamero M, Pio DT, Tarelho LAC, Sánchez P, Sanchez-Silva L. Simulation of biomass gasification in bubbling fluidized bed reactor using aspen plus®. Energy Convers Manag 2021;235:113981.

[47] Kaushal P, Tyagi R. Advanced simulation of biomass gasification in a fluidized bed reactor using ASPEN PLUS. Renew Energy 2017;101:629–36.

[48] Benali M, Shakourzadeh-Bolouri K. The gas-solid-solid packed contactor: Hydrodynamic behaviour of counter-current trickle flow of coarse and dense particles with a suspension of fine particles. Int J Multiph Flow 1994;20:161–70.

[49] Ergun circulating fluid beds. Fluidbed reactor design parameters. http://www.utc.fr/ergun/ergun_cfb.html [accessed 02/03/2021]

[50] George SE, Grace JR. Entrainment of particles from a pilot scale fluidized bed. Can J Chem Eng 1981;59:279–84.

[51] George SE, Grace JR. Heat transfer to horizontal tubes in the freedboard region of a gas fluidized bed.

AIChE J 1982;28:759–65.

[52] Geldart D. The effect of particle size and size distribution on the behaviour of gas-fluidised beds. Powder Technol 1972;6:201–15.

[53] Geldart D, Baeyens J. The design of distributors for gas-fluidized beds. Powder Technol 1985;42:67–78.

[54] Geldart D, Harnby N, Wong AC. Fluidization of cohesive powders. Powder Technol 1984;37:25–37.

[55] Geldart D, Wong ACY. Fluidization of powders showing degrees of cohesiveness—II. Experiments on rates of de-aeration. Chem Eng Sci 1985;40:653–61.

[56] Seider WD, Seader JD, Lewin DR. Product & process design principles: synthesis, analysis and evaluation, (with cd) John Wiley & Sons; 2009.

[57] Max PX. Equipment Cost for Chemical Engineers. McGraw-Hill High Educ n.d. http://www.mhhe.com/engcs/chemical/peters/data/. [Accessed on 25/01/2020]

[58] Matches M. Equipment Cost Estimator. Matches' 275 Equip Cost Estim n.d. https://www.matche.com/equipcost/. [Accessed on 25/01/2020].

[59] Peters MS, Timmerhaus KD, others. Plant design and economics for chemical engineers McGraw-Hill Inc., United States, 1980.

[60] Rahbari A, Shirazi A, Venkataraman MB, Pye J. A solar fuel plant via supercritical water gasification integrated with Fischer--Tropsch synthesis: Steady-state modelling and techno-economic assessment. Energy Convers Manag 2019;184:636–48.

[61] Ramirez JA, Brown R, Rainey TJ. Techno-economic analysis of the thermal liquefaction of sugarcane bagasse in ethanol to produce liquid fuels. Appl Energy 2018;224:184–93.

[62] Reserve bank of Australia. RB. Exchange Rates. Reserv Bank Aust 2020. https://www.rba.gov.au/statistics/frequency/exchange-rates.html [Accessed 20/06/2021]

[63] Purity Gas, Canada. Nitrogen Generation for Chemical Industries. Purity Gas 2020. https://puritygas.ca/nitrogen-generation-for-chemical-industry [accessed on 15/09/2021] [64] Gas Price Trends Review Report, V2.1. EnergyGovAu n.d, 2017. Oakley Greenwood. https://www.energy.gov.au [Accessed on 04/07/2021]

[65] Musa M, Doshi A, Brown R, Rainey TJ. Microalgae dewatering for biofuels: A comparative techno-economic assessment using single and two-stage technologies. J Clean Prod 2019;229:325–36.

[66] EIA US. Levelized cost and levelized avoided cost of new generation resources in the annual energy outlook 2016. Washington DC, USA 2016.

[67] Doshi A, Pascoe S, Coglan L, Rainey T. The financial feasibility of microalgae biodiesel in an integrated, multi-output production system. Biofuels, Bioprod Biorefining 2017;11:991–1006.

[68] Dorris CC, Lu E, Park S, Toro FH. High-purity oxygen production using mixed ionic-electronic conducting sorbents 2016.

[69] Rodriguez JM, Sánchez D, Martinez GS, Ikken B, others. Techno-economic assessment of thermal energy storage solutions for a 1 MWe CSP-ORC power plant. Sol Energy 2016;140:206–18.

[70] Comello SD, Glenk G, Reichelstein S. Levelized cost of electricity calculator: A user guide. Sustain Energy Initiat 2017.

[71] Rhodes NR, Bobek MM, Allen KM, Hahn DW. Investigation of long term reactive stability of ceria for use in solar thermochemical cycles. Energy 2015;89:924–31.

[72] Bailey MP. Chemical Engineering Magazine, URL:http://www.chemengonline.com/Chemical Engineering; New York Vol. 126, Issue. 3, (March 2019) Chem Eng - Chem Eng Essentials Glob Chem Process Ind 2020.

[73] Bailey MP. Chemical Engineering Magazine, URL:http://www.chemengonline.com/ Chemical Engineering; New York Vol. 123, Issue. 3, (Mar 2016): 92. Chem Eng - Chem Eng Essentials Glob Chem Process Ind 2020.

[74] Oxygen global market price. Price Conversions Cost Calc Mater Subst n.d. https://www.aqua-calc.com/calculate/materials-price [accessed on 06/09/2021]

[75] Forecasting scenarios, methodologies and inputs. AEMO n.d. Australian Energy Market Operator, 2019. www.aemo.com.au/Files/NEM/Input_Assumptions_Methodologies [Accessed on 06/05/2021]

[76] United States Environmental protection agency, EPA carbon emission cost estimate https://www.epa.gov/energy/greenhouse-gases-equivalencies-calculator-calculations-and-references [accessed on 08/09/2021]

[77] Bureau of Meteorology. Climate information for solar energy. Clim Inf Sol Energy, Bur Meteorol n.d. http://www.bom.gov.au/climate/data-services/solar-information.shtml [accessed on 25/01/2021] [78] Falter C, Sizmann A. Solar Thermochemical Hydrogen Production in the USA. Sustainability 2021;13:7804.

[79] Falter C, Valente A, Habersetzer A, Iribarren D, Dufour J. An integrated techno-economic, environmental and social assessment of the solar thermochemical fuel pathway. Sustain Energy \& Fuels 2020;4:3992–4002.

[80] Khodabandehloo M, Larimi A, Khorasheh F. Comparative process modeling and techno-economic evaluation of renewable hydrogen production by glycerol reforming in aqueous and gaseous phases. Energy Convers Manag 2020;225:113483.

[81] Majumdar A, Deutch JM, Prasher RS, Griffin TP. A framework for a hydrogen economy. Joule 2021;5:1905–8.

[82] Ajanovic A, Haas R. Prospects and impediments for hydrogen and fuel cell vehicles in the transport sector. Int J Hydrogen Energy 2021;46:10049–58.

[83] Sharma P, Gallagher B, Sultoon J. Green pivot: can Australia master the hydrogen trade? APPEA J 2021;61:466–70.